# Cluster simulations in the Gross Neveu model

DIPLOMARBEIT

zur Erlangung des akademischen Grades
Diplom-Physiker
(Dipl.-Phys.)
im Fach Physik

eingereicht an der
Mathematisch-Naturwissenschaftlichen Fakultät I
Humboldt-Universität zu Berlin

von
Herr Willi Rath

Präsident der Humboldt-Universität zu Berlin:
Prof. Dr. Dr. h.c. Christoph Markschies

Dekan der Mathematisch-Naturwissenschaftlichen Fakultät I:
Prof. Dr. Lutz-Helmut Schön

Gutachter:

1. Prof. Dr. Ulli Wolff
2. Prof. Dr. Michael Müller-Preussker

eingereicht am: 14. Januar 2009

**Abstract**

This thesis reports on testing of a global algorithm for Majorana Wilson fermions on a one plus one dimensional space time lattice. The fermions fields are coupled with a quartic interaction known as the Gross Neveu interaction. The model is expressed in terms of dimer variables which live on the links. A global algorithm, the loop gas, or fermion cluster algorithm, is derived. The Green's functions, and especially the scalar correlation are introduced. Two definitions of the critical point are compared in the infinite volume limit. The critical line is measured and compared to leading order perturbation theory. The large $N$ limit is discussed, and symmetry breaking of the effective potential is observed for a finite number of flavors. The part of the parameter space which is covered by the algorithm is examined. The computational effort necessary to simulate on large lattices is estimated.

**Keywords:**
Gross Neveu model, Majorana Wilson fermions, Monte Carlo, Lattice field theory

**Zusammenfassung**

Diese Arbeit beschreibt Tests eines globalen Algorithmus' für Majorana-Wilson-Fermionen auf einem 1+1-dimensionalen Raumzeitgitter. Die Fermionfelder werden über eine quartische Wechselwirkung, welche als Gross-Neveu-Wechselwirkung bekannt ist, gekoppelt. Die Wirkung wird in Dimer-Variablen, welche auf den Verbindungen zwischen den Gitterpunkten leben, ausgedrückt. Anschließend wird der "Loop-Gas"-Algorithmus, oder auch "Fermion-Cluster"-Algorithmus, abgeleitet. Green'sche Funktionen, insbesondere die skalare Korrelationsfunktion, werden eingeführt. Zwei verschiedene Definitionen für den kritischen Punkt werden im Limes unendlichen Volumens miteinander verglichen. Die kritische Linie wird bestimmt und mit der führenden Ordnung der Störungstheorie verglichen. Der Limes unendlich vieler Flavors wird diskutiert. Für endlich viele Flavors wird die Symmetriebrechung des effektiven Potentials beobachtet. Der Teil des Parameterraumes, der mit dem Algorithmus behandelt werden kann, wird eingegrenzt. Die Rechenzeit, die nötig ist, um große Gitter zu simulieren, wird abgeschätzt.

**Schlagwörter:**
Gross-Neveu-Modell, Majorana-Wilson-Fermionen,
Monte-Carlo-Simulation, Gitter-Feldtheorie

# Contents

# Introduction

This thesis reports on testing of an algorithm for Monte Carlo simulations of two-dimensional interacting fermions. Its goal was to use a C version of a recently proposed global algorithm [1] for the two dimensional Gross Neveu model [2], to perform measurements with large statistics.

The Gross Neveu model is a two dimensional fermionic field theory with a quartic interaction. It has been proposed in 1974 [2]. The model shows dynamical symmetry breaking, it has a spectrum of bound states[3, 4], it is asymptotically free, and there is a large $N$ expansion (number of flavors) [2, 5–7]. The Gross Neveu model with two flavors of Majorana fermions (one flavor of Dirac fermions) is equivalent to the Thirring model [8, 9].

In particle physics as well as in solid state physics, Monte Carlo simulations of fermions play an important role. However, simulations of fermions face many obstacles. One of them is due to the fact that it is not possible to directly sample the Grassmannian variables which represent fermionic fields in the path integral approach. This problem can be accounted for by parameterizing Grassmann integrals in terms of polymers [10, 11]. Another obstacle is known as the sign problem. Oscillating signs of the weights in the path integral representation of fermions result in Monte Carlo errors which grow exponentially with the lattice volume [12]. For two-dimensional fermions, the sign problem can be solved with the algorithm used in this work [1].

In the first chapter of this thesis, the action of Gross Neveu model is introduced in terms of Majorana fermions, and its discretization with Wilson fermions is discussed. The second chapter presents the loop gas algorithm for the free case, and for the interacting theory.

The third chapter is on observables. The Green's function of the Dirac operator. Variables which are naturally used in the update process, and which are thus computationally very cheap observables are discussed.

In chapter four, the algorithm is tested for the free case. Two observables which are connected to the two point functions of the fermionic fields are

measured, and the sensitivity of the algorithm to the quality of the random numbers that are used in the Monte Carlo update are examined.

The fifth chapter examines tuning to the critical point. Two different definitions of the critical mass are compared in the infinite volume limit. The critical line is measured and compared to perturbation theory predictions.

Chapter six describes the limit of infinitely many flavors. The effective potential is shown to undergo a transition to a phase of broken symmetry at a critical lattice size. The effect of this symmetry breaking is also measured for a finite number of flavors.

The last chapter discusses the limitations of the algorithm. The first appendix contains a list of the various ensembles used in this thesis. The second appendix presents the data from the measurement of the critical line.

# Chapter 1

# The Gross Neveu model

The Gross Neveu model is defined. Then, after a brief overview of the symmetries of the Lagrangian, the model is discretized in terms of Wilson fermions. The free Wilson propagator and the scalar time slice correlation function are introduced.

## 1.1 Action and symmetries of the Gross Neveu model

The Gross Neveu model describes fermions in a one plus one dimensional space time which are coupled by a quartic interaction. It was proposed in 1974 to study dynamical symmetry breaking of an asymptotically free theory [2]. In this work the model will be expressed in terms of $N$ flavors of Majorana fermions [1, 13] which are coupled by a quartic interaction. The Euclidean continuum action reads

$$S = \int \mathrm{d}^2x \left[ \frac{1}{2} \xi^T(x) \mathcal{C} \left( \not{\partial} + m \right) \xi(x) - \frac{g^2}{8} \left( \xi^T(x) \mathcal{C} \xi(x) \right)^2 \right] . \tag{1.1}$$

The full index structure of the fermion field is $\xi_{ai}(x)$ with the spinor index $a = 0, 1$ and the flavor index $i = 1, \ldots, N$. The interaction term of (1.1) is, for example, an abbreviation for

$$\frac{g^2}{2} \left( \sum_{iab} \xi_{ai}(x) \mathcal{C}_{ab} \xi_{bi}(x) \right)^2 . \tag{1.2}$$

and thus couples different flavors. The charge conjugation operator $\mathcal{C}$ fulfills

$$\mathcal{C} \gamma_\mu \mathcal{C}^{-1} = - \gamma_\mu^T \qquad\qquad \mathcal{C} = - \mathcal{C}^T . \tag{1.3}$$

Whenever the representation is needed explicitly, the Dirac matrices are chosen to

$$\gamma_0 = \sigma_3 = \begin{pmatrix} 1 & 0 \\ 0 & -1 \end{pmatrix} \qquad \gamma_1 = \sigma_1 = \begin{pmatrix} 0 & 1 \\ 1 & 0 \end{pmatrix} . \tag{1.4}$$

Then, a proper choice in two dimensions is

$$\mathcal{C} = \mathrm{e}^{-i\alpha}\gamma_0\gamma_1 = -i\mathrm{e}^{-i\alpha}\gamma_5 \tag{1.5}$$

where $\alpha$ is an arbitrary phase [14].

The Gross-Neveu action has a global $\mathcal{O}(N)$ invariance

$$\xi(x) \longrightarrow M\xi(x), \quad M \in \mathcal{O}(N) \tag{1.6}$$

which is manifest in the Majorana notation. For the massless case there is a chiral symmetry

$$\xi(x) \longrightarrow \gamma_5\xi(x), \tag{1.7}$$

where $\gamma_5$ obeys

$$[\mathcal{C}, \gamma_5] = 0 \qquad \{\gamma_\mu, \gamma_5\} = 0 . \tag{1.8}$$

Discretizing the model in terms of Wilson fermions will explicitly break the chiral symmetry even if the mass vanishes.

## 1.2 Discretization in terms of Wilson fermions

The simplest way to discretize the action (1.1) would be to replace the slashed derivative by a finite difference operator, and to consider the two-dimensional space time as a torus which periodically continues the time and the space directions with a length $T$ and $L$ respectively. This naïve approach results in free ($g^2 = 0$) energies [15]

$$E_q = \pm\sqrt{m^2 + a^{-2}\sin^2 q} \tag{1.9}$$

where the $q$ are the momenta

$$q = 0, \frac{2\pi}{L}, \ldots, \frac{2\pi(L-1)}{L} . \tag{1.10}$$

As the squared sine is periodic with respect to shifts by multiples of $\pi$, the energies are degenerate

$$E_q = E_{q+\pi} . \tag{1.11}$$

Consequently, there is an extra fermion state belonging to $q+\pi$, which stems from the lattice discretization but survives in the continuum limit. This second state will influence the results of lattice calculations in a nontrivial way.

The unwanted extra fermion can be removed by introducing an extra momentum dependent mass term, the Wilson term, which is proportional to the lattice spacing and hence does not change the continuum limit of the action. The action discretized in terms of Wilson fermions [1] reads

$$S = a^2 \sum_x \left[ \frac{1}{2} \xi^T \mathcal{C} \left( \tilde{\not\partial} + m - \frac{ra}{2} \partial^* \partial \right) \xi - \frac{g^2}{8} (\xi^T \mathcal{C} \xi)^2 \right] . \tag{1.12}$$

The corresponding free fermion energies are then

$$E_q = \pm \sqrt{\left( m + \frac{r}{a}(1 - \cos q) \right)^2 + a^{-2} \sin^2 q} \tag{1.13}$$

and shifting the momenta by $\pi$ results in

$$E_{q+\pi} = E_q \Big|_{m \to m + 2r/a} . \tag{1.14}$$

The extra fermion states acquire an infinitely large mass if $a \to 0$ and do not contribute in the continuum limit.

That part of the action (1.12) which couples the nearest neighbor Majorana fields can be rewritten in terms of Wilson projectors

$$P(n) = \frac{1 - \not{n}}{2} . \tag{1.15}$$

Setting the lattice spacing $a$ and the Wilson parameter $r$ to one[1], and using the symmetric, forward, and backward discretized nearest neighbor deriva-

[1] The substitution $\sqrt{a}\xi \to \xi$ and $a\,m \to m$ renders the mass and the fields dimensionless.

tives[2] $\tilde{\partial}_\mu$, $\partial_\mu$, and $\partial^*_\mu$ the action reads

$$\begin{aligned} S = \frac{1}{2} \sum_x \underbrace{(2+m)}_{\equiv\varphi} \xi^T(x)\mathcal{C}\xi(x) \\ - \sum_{x,\mu} \xi^T(x)\mathcal{C}P(\hat{\mu})\xi(x+\hat{\mu}) \\ - \frac{g^2}{8} \sum_x \left(\xi^T(x)\mathcal{C}\xi(x)\right)^2 \ . \end{aligned} \tag{1.16}$$

Here, the abbreviation $\varphi = 2+m$ was introduced. Later, $\varphi$ will be considered as an external $x$-dependent field.

### 1.2.1 Boundary conditions

On a finite lattice of the size $T \times L$, it is necessary to define the boundary conditions explicitly. Here the time and the space direction will be continued periodically or anti-periodically. The boundary conditions will be denoted by the two component vector

$$\epsilon = (\epsilon_0, \epsilon_1) \in \{(0,0);(1,0);(0,1);(1,1)\} \tag{1.17}$$

where $\epsilon_i = 0$ means periodicity and $\epsilon_i = 1$ means anti-periodicity in the $i$-direction. This (anti-)periodicity applies for the fields $\xi$. With $L_\mu = T, L$ for $\mu = 0, 1$, the fields obey

$$\xi(x \pm \hat{\mu} \cdot L_\mu) = (-1)^{\epsilon_\mu} \xi(x) \tag{1.18}$$

whereas bilinear quantities are always periodic

$$\xi_{ai}(x \pm \hat{\mu} \cdot L_\mu)\xi_{bj}(y \pm \hat{\mu} \cdot L_\mu) = \xi_{ai}(x)\xi_{bj}(y) \ . \tag{1.19}$$

[2] The discrete derivatives are (with $a = 1$)

$$\begin{aligned} 2\tilde{\partial}_\mu f(x) &= f(x+\hat{\mu}) - f(x-\hat{\mu}) \\ \partial_\mu f(x) &= f(x+\hat{\mu}) - f(x) \\ \partial^*_\mu f(x) &= f(x) - f(x-\hat{\mu}) \\ \Rightarrow \ \partial^*\partial f(x) &= \sum_\mu [f(x+\hat{\mu}) + f(x-\hat{\mu}) - 2f(x)] = \partial\partial^* f(x) \ . \end{aligned}$$

### 1.2.2 Wilson propagators for the free case

The free ($g^2 = 0$) propagator $G$ is defined by

$$\langle \xi_{ai}(x)\xi_{bj}\rangle_0 = \delta_{ij}\left[G(x-y)\mathcal{C}^{-1}\right]_{ab} \tag{1.20}$$

and obeys

$$\left(\gamma_\mu \tilde{\partial}_\mu + m - \frac{1}{2}\partial^*\partial\right) G(x) = \delta_{x,0} = \delta_{x_0,0}\delta_{x_1,0} \ . \tag{1.21}$$

In momentum space (1.21) is an algebraic equation with the solution

$$\tilde{G}(p) = \frac{-i\mathring{\not{p}} + M}{\mathring{p}^2 + M^2} \qquad\qquad G(x) = \frac{1}{TL}\sum_p \mathrm{e}^{ipx}\tilde{G}(p) \ , \tag{1.22}$$

where the following short cuts were used:

$$\mathring{p}_\mu = \sin p_\mu \qquad \hat{p}_\mu = 2\sin\frac{p_\mu}{2} \qquad M = m + \frac{1}{2}\hat{p}^2 \ . \tag{1.23}$$

The momenta depend on the boundary conditions:

$$p = (p_0, p_1) = \left(\frac{2\pi}{T}\left[n_0 + \frac{\epsilon_0}{2}\right], \frac{2\pi}{L}\left[n_1 + \frac{\epsilon_1}{2}\right]\right)$$
$$n_0 = 0, \ldots, T-1 \qquad n_1 = 0, \ldots, L-1 \ .$$

### 1.2.3 Chiral symmetry and critical mass

The Wilson term $-ra/2\partial^*\partial$ breaks the chiral symmetry

$$\xi \to \gamma_5 \xi \tag{1.24}$$

of the continuum action (1.1) even if $m = 0$. If the continuum is approached, the chirally symmetry is restored for a critical mass $m_c(g^2)$. For a fixed coupling $g^2$, the critical mass can be determined with a quantity that vanishes due to chiral symmetry. As the scalar correlation $\langle \xi^T \mathcal{C}\xi\rangle$ changes sign under the chiral transformation (1.7),

$$\langle \xi(y)^T \gamma_5^T \mathcal{C}\gamma_5 \xi(x)\rangle = \langle \xi(y)^T(-\mathcal{C})\xi(x)\rangle = -\langle \xi(y)^T\mathcal{C}\xi(x)\rangle \ . \tag{1.25}$$

In [13] and in [14], the scalar time slice correlation correlation was used to define the critical mass. In chapter 5, a similar quantity will be used to tune the mass to its critical value.

# Chapter 2

# The loop gas algorithm

The Wilson fermion Gross Neveu model is rewritten in terms of variables $k$ that live on the links and that can only assume the values 0 or 1. The links are said to host a dimer if $k = 1$ and to be empty otherwise. The dimers will have to obey constraints forcing them to form closed non-intersecting and non-backtracking loops. In [16] a local (plaquette by plaquette) update for these loops was discussed. The global algorithm presented in [1, 17] is used in this work.

The algorithm is derived on a two dimensional lattice of the size $T \times L$. Sites are denoted by $x = (x_0, x_1)$ where the index 0 refers to the time and the index 1 refers to the space direction. The lattice is closed around a torus. In both directions the boundary conditions (of the fields), denoted by $\epsilon = (\epsilon_0, \epsilon_1)$, can be chosen to be periodic ($\epsilon_i = 0$) or anti-periodic ($\epsilon_i = 1$).

## 2.1 The loop ensemble for free Wilson fermions

First, free Wilson fermions are rewritten in terms of dimer variables which live on the links. These dimer variables have to obey constraints forcing them to form closed, non-intersecting, and non-backtracking loops. Then, the modulus of the weight of an allowed dimer configuration is found to depend only on local properties of the dimer field (the number of "corners"), and on the now $x$-dependent auxiliary field $\varphi(x)$. The sign of a dimer configuration depends on the global structure (parameterized by the topology) of the configuration, and on the boundary conditions.

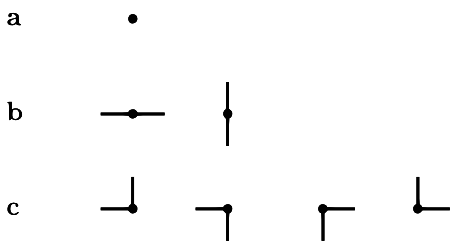


**Figure 2.1:** Allowed site configurations. The dot represents a site, and the lines represent the dimers attached to the site. From these building blocks, only closed loops that do not intersect or backtrack can be build. An intersecting loop would contain a site with four dimers and a backtracking loop would contain sites with more than one dimers.

### 2.1.1 Introducing the dimers into the partition function

The partition function for Majorana Wilson fermions[1]

$$Z_\xi^\epsilon[\varphi] = \int \mathrm{D}\xi \mathrm{e}^{\frac{1}{2}\sum\limits_x \varphi(x)\xi^T(x)\mathcal{C}\xi(x) - \sum\limits_{x,\mu} \xi^T(x)\mathcal{C}P(\hat{\mu})\xi(x+\hat{\mu})} \tag{2.1}$$

can be completely expressed in terms of variables that live on the links between the sites. With

$$\left[\xi^T(x)\mathcal{C}P(\hat{\mu})\xi(x+\hat{\mu})\right]^k = 0 \quad \text{for} \quad k > 1 \tag{2.2}$$

that part of the exponential that contains the Wilson projectors can be expanded into a series which may be truncated after the linear term. The exponent represents an empty link if $k_{x,\mu} = 0$ and a dimer if $k_{x,\mu} = 1$. The link is said to connect the site $x$ with its nearest neighbor $x + \hat{\mu}$ if it hosts a dimer. Sites that have no adjacent dimers will be called *monomers*.

The partition function contains all possible $2^{2V}$ dimer configurations[2]

$$Z_\xi^\epsilon[\varphi] = \sum_{\{k_{x,\mu}=0,1\}} \int \mathrm{D}\xi \mathrm{e}^{-\frac{1}{2}\sum\limits_x \varphi\xi^T\mathcal{C}\xi} \prod_{x,\mu} \left[\xi^T(x)\mathcal{C}P(\hat{\mu})\xi(x+\hat{\mu})\right]^{k_{x,\mu}} \quad . \tag{2.3}$$

[1] Now the field $\varphi(x) = 2 + m(x)$, or the mass respectively, is considered $x$-dependent. Later, the auxiliary field $\varphi(x)$ will be used to couple $N$ flavors of Wilson fermions (see section 2.3). The superscript $\epsilon$ denotes the boundary conditions (see section 1.2.1).

[2] The set of $k_{x,\mu}$ for all sites $x$, and for all forward directions $\mu$ is called dimer configuration. The field $k$ is called dimer field.

Not all dimer configurations have a non-vanishing weight. From the Grassmann integrals[3]

$$\varphi = \int \mathrm{d}^2\xi(x) \mathrm{e}^{-\frac{1}{2}\varphi(x)\xi(x)^T\mathcal{C}\xi(x)} \tag{2.4}$$

$$0 = \int \mathrm{d}^2\xi(x) \mathrm{e}^{-\frac{1}{2}\varphi(x)\xi(x)^T\mathcal{C}\xi(x)}\xi_a(x) \tag{2.5}$$

$$\mathcal{C}^{-1}_{ab} = \int \mathrm{d}^2\xi(x) \mathrm{e}^{-\frac{1}{2}\varphi(x)\xi(x)^T\mathcal{C}\xi(x)}\xi_a\xi_b \ , \tag{2.6}$$

$$\tag{2.7}$$

and from

$$0 = \xi(x)_a\xi(x)_b\xi(x)_c = \xi(x)_a\xi(x)_b\xi(x)_c\cdots \tag{2.8}$$

it is evident that only those configurations which contain zero or two dimers adjacent to every site contribute to $Z^{\epsilon}_{\xi}$.

Since dimers always connect one site to another, only configurations that consist of monomers and of non-intersecting, non-backtracking closed loops of dimers can occur. The building blocks from which all possible dimer configurations can be assembled are displayed in figure 2.1. An intersecting loop would contain at least one site with four dimers. A backtracking loop would contain at least one link with two dimers (or $k = 2$) and is forbidden by $P(\hat{n})P(-\hat{n}) = 0$. Open chains of dimers would contain sites with only a single dimer at their ends and hence are also forbidden.

### 2.1.2 Contributions from the monomers

With the Grassmann integrals (2.4) and (2.6), the partition function (2.3) factorizes into contributions from the monomers, and from the dimer loops. The contribution from the monomers is

$$\prod_{x\in\{\text{monomers}\}} \varphi(x) \ . \tag{2.9}$$

Every monomer contributes the value of the scalar field $\varphi$ at its site.

### 2.1.3 Contributions from the dimer loops

To calculate the dimer loop contributions, more work is necessary. For simplicity, the boundary conditions are considered to be periodic ($\epsilon = (0, 0)$).

[3]The arbitrary phase of the charge conjugation operator has been explicitly chosen to $\mathcal{C} = -i\gamma_5 = \begin{pmatrix} 0 & 1 \\ -1 & 0 \end{pmatrix}$.

Later it will be easy to restore general boundary conditions again. As a starting point a loop that contains subsequent sites connected by the unit vectors $\hat{n}_i$ is considered. For definiteness the loop will be traced in an explicit direction starting from an explicit site both of which will eventually be irrelevant for the loop contribution. This loop will be denoted by

$$\Gamma \leftrightarrow (\hat{n}_1, \ldots, \hat{n}_l) \ . \tag{2.10}$$

After contracting the spinor indices of all factors connected by (2.6) the contribution of the dimer loop $\Gamma$ amounts to a factor

$$X(\Gamma) = -\operatorname{tr}[P(\hat{n}_1) \cdots P(\hat{n}_l)] \ . \tag{2.11}$$

**Direction and starting point of the loop**

Traces are invariant under cyclic shifts and hence $X(\Gamma)$ is independent of the starting point of the loop. The $\gamma_\mu$ and all products of an odd number of $\gamma_\mu$ are traceless. Therefore, $X$ only contains combinations of an even number of $\hat{n}_i$, and flipping the signs of *all* the $\hat{n}_i$ does not change $X$:

$$X(\hat{n}_1, \ldots, \hat{n}_l) = X(-\hat{n}_1, \ldots, -\hat{n}_l) \ . \tag{2.12}$$

Finally, with $\mathcal{C}\gamma_\mu\mathcal{C}^{-1} = -\gamma_\mu^T$, and with $\mathcal{C}P(\hat{n})\mathcal{C}^{-1} = P(-\hat{n})^T$

$$\begin{aligned} \operatorname{tr}[P(\hat{n}_1) \cdots P(\hat{n}_l)] &= \operatorname{tr}[\mathcal{C}P(\hat{n}_1)\mathcal{C}^{-1} \cdots \mathcal{C}P(\hat{n}_l)\mathcal{C}^{-1}] \\ &= \operatorname{tr}[P(-\hat{n}_1)^T \cdots P(-\hat{n}_l)^T] \\ &= \operatorname{tr}[\{P(-\hat{n}_l) \cdots P(-\hat{n}_1)\}^T] \\ &= \operatorname{tr}[P(-\hat{n}_l) \cdots P(-\hat{n}_1)] \ , \end{aligned} \tag{2.13}$$

and thus the loop contribution does not depend on the direction of its evaluation

$$X(\hat{n}_1, \ldots, \hat{n}_l) = X(-\hat{n}_l, \ldots, -\hat{n}_1) \ . \tag{2.14}$$

**Corners and winding number of the loop**

From here on it is assumed that the idempotency of the projectors

$$P(\hat{n})P(\hat{n}) = P(\hat{n}) \tag{2.15}$$

has already been applied to remove all redundant $P(\hat{n}_i)$ from $X$ (except maybe for the pair $P(\hat{n}_1)$, $P(\hat{n}_l)$). Then, the loop only consists of corners and at most one straight piece, where the first and last dimer meet.

Before the trace will eventually be evaluated, it is noted that *orthonormal* spinors $\not{m}$ and $\not{n}$ can be rotated into each other by

$$\not{m} = R(\hat{m},\hat{n})\not{n}R(\hat{m},\hat{n})^{-1} \tag{2.16}$$

with[4]

$$R(\hat{m},\hat{n}) = \mathrm{e}^{\frac{\pi}{8}[\not{m},\not{n}]} = \mathrm{e}^{\frac{\pi}{4}\not{m}\not{n}} = \frac{1}{\sqrt{2}}(1+\not{m}\not{n}) \ . \tag{2.17}$$

The transformation also applies for the projectors

$$P(\hat{m}) = R(\hat{m},\hat{n})P(\hat{n})R(\hat{m},\hat{n})^{-1} \ , \tag{2.18}$$

and hence the products of projectors can be build out of a sequence of rotations acting on the last projector in the product. The minimal building block is

$$\begin{aligned} P(\hat{n}_1)P(\hat{n}_2) &= R(\hat{n}_1,\hat{n}_2)\underbrace{P(\hat{n}_2)R(\hat{n}_1,\hat{n}_2)^{-1}P(\hat{n}_2)}_{=\frac{1}{\sqrt{2}}P(\hat{n}_2)} \\ &= \frac{1}{\sqrt{2}}R(\hat{n}_1,\hat{n}_2)P(\hat{n}_2) \ , \end{aligned} \tag{2.19}$$

and iteration leads to

$$P(\hat{n}_1)\cdots P(\hat{n}_l) = \left(\frac{1}{\sqrt{2}}\right)^{l-1} R(\hat{n}_1,\hat{n}_2)\cdots R(\hat{n}_{l-1},\hat{n}_l)P(\hat{n}_l) \ . \tag{2.20}$$

The rotation which transforms $\not{n}$ once along the whole loop is

$$R_\Gamma = R(\hat{n}_1,\hat{n}_2)\cdots R(\hat{n}_{l-1},\hat{n}_l)R(\hat{n}_l,\hat{n}_1) \ , \tag{2.21}$$

and consequently,

$$X(\Gamma) = -\left(\frac{1}{\sqrt{2}}\right)^{l-1} \mathrm{tr}[R_\Gamma R(\hat{n}_1,\hat{n}_l)P(\hat{n}_l)] \ . \tag{2.22}$$

For $R_\Gamma$ two cases are possible. Either the loop winds around the torus and all the rotations cancel to $R_\Gamma = +1$, or, by changing only single plaquettes[5], the loop can be contracted to a single plaquette, and $R_\Gamma = -1$, because rotating a spinor by $2\pi$ yields a minus sign. The sign of $R_\Gamma$ can be expressed in terms of the winding number $w$ which counts how many times the loop winds around the torus in either direction. $w = 0$ corresponds to no winding,

[4]For orthonormal spinors $\not{m}$ and $\not{n}$: $\exp[\alpha\not{m}\not{n}] = \cos\alpha + \not{m}\not{n}\sin\alpha$.

[5]The topology of the loops will be discussed in detail later.

and $w = 1, 2$ corresponds to winding in one or in both directions respectively. Altogether,

$$R_\Gamma = (-1)^{w+1} \ . \tag{2.23}$$

The remaining trace can be explicitly evaluated for the relevant cases

$$\mathrm{tr}[R(\hat{n}_1, \hat{n}_l)P(\hat{n}_l)] = \begin{cases} 1 & \text{for } \hat{n}_1 = \hat{n}_l \ , \\ \frac{1}{\sqrt{2}} & \text{for } \hat{n}_1 \perp \hat{n}_l \ , \end{cases} \tag{2.24}$$

where the definition of $R$ and $P$ and $\mathrm{tr}[\gamma_\mu] = 0$ were used.

**Contribution from the loop**

Finally, since $l$ (or $l - 1$ for $\hat{n}_1 = \hat{n}_l$) is the number of corners $N_c$ (see figure 2.1.c) of the dimer loop,

$$X = \left(\frac{1}{\sqrt{2}}\right)^{N_c} (-1)^w \ . \tag{2.25}$$

Later, the sign of (2.25) will be determined by the boundary conditions and by the topology of the loops in such a way that a loop winding around the torus in an anti-periodic direction picks up an extra minus sign. If there is more than one loop in the configuration, the contributions from all the loops, and the contribution from the monomers multiply.

### 2.1.4 Topologies the dimer loops and of dimer configurations

On the torus, four classes of dimer loops can be defined. Each class contains only loops that can be transformed into each other by a sequence of flipping[6] all dimers of single plaquettes. Loops that belong to the same class are said to be *homotopic* to each other. The topologies are denoted by a two component vector

$$e = (e_0, e_1) \in \{(0,0); (1,0); (0,1); (1,1)\} \tag{2.26}$$

with $e_i = 1$ denoting loops homotopic to one winding in direction $i$ and $e_i = 0$ denoting loops homotopic to no winding in direction $i$. Loops with $e = (0,0)$ are homotopic to the trivial configuration which only consists of monomers. Loops from the classes $e = (1,0)$, or $e = (0,1)$ are homotopic to one straight line winding around the temporal or spatial direction respectively, and loops with $e = (1,1)$ are homotopic to a loop winding around both directions simultaneously.

[6] $k = 1 \leftrightarrow k = 0$

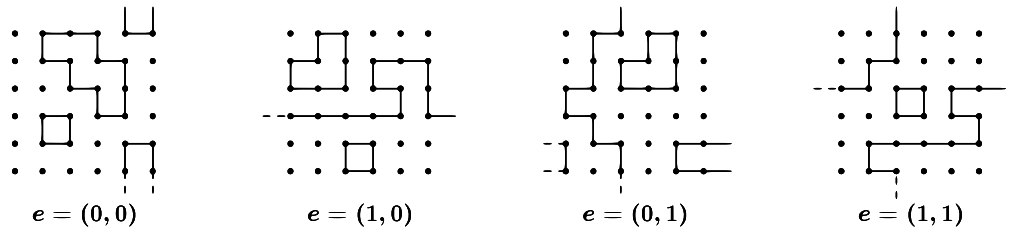


**Figure 2.2:** Topologies of the dimer loops. $e = (0, 0)$ refers to no winding around the torus, $e = (1, 0)$ [$e = (0, 1)$] denotes one winding in the time [space] direction, and $e = (1, 1)$ means winding once in each of the two directions.

If there are many loops in a configuration, their topology is determined by summing the topologies $e$ of all of them modulo 2. In figure 2.2 typical configurations for all four topologies are displayed. For example, two lops with $e = (0, 0)$ each together with one loop with $e = (1, 0)$ make a configuration with $e = (1, 0)$.

With the topology $e$, the sign of (2.25) which is due to the full rotation of a spinor can be rewritten to

$$(-1)^w = 2\delta_{e,0} - 1 \ . \tag{2.27}$$

### 2.1.5 Boundary conditions and the sign of the dimer loop contribution

Now, the boundary conditions $\epsilon$ can be restored. If a loop winds once around direction $i$, the contribution of that loop gets an extra minus sign if the direction $i$ is anti-periodic. Therefore, loops that have the topology $e$ get $e \cdot \epsilon$ minus signs from anti-periodicity. Note that a configuration which consists of two loops winding around the same direction belong to the class $e = (0, 0)$. This is consistent with the fact that this configuration gets two canceling minus signs. Altogether the contribution from all the dimer loops in one configuration is

$$X = \left(\frac{1}{\sqrt{2}}\right)^{N_c} (-1)^{\epsilon \cdot e}(2\delta_{e,0} - 1) \ . \tag{2.28}$$

### 2.1.6 Summary: the loop ensemble

Collecting (2.9) and (2.28) the partition function (2.3) can be expressed in terms of positive weights $\rho[k; \varphi]$ depending on the dimer configuration $k$, and on the $x$-dependent mass $\varphi(x) = 2 + m(x)$ times a sign $\Phi[e(k); \epsilon]$ stemming from the topology of the dimer configuration, and from the boundary

conditions:

$$Z_\xi^\epsilon[\varphi] = \sum_{\{k_{x,\mu}\}} \rho[k;\varphi]\, \Phi[e(k);\epsilon] \tag{2.29}$$

$$\Phi[e(k);\epsilon] = (-1)^{\epsilon\cdot e}(2\delta_{e,0} - 1) \tag{2.30}$$

$$\rho[k;\varphi] = \prod_x f_x(k,\varphi) \tag{2.31}$$

$$f_x(k,\varphi) = \begin{cases} \varphi(x) & \text{no dimer at } x, \\ 1 & \text{two collinear dimers at } x, \\ \frac{1}{\sqrt{2}} & \text{two orthogonal dimers at } x, \\ 0 & \text{else.} \end{cases} \tag{2.32}$$

In the next section an algorithm which samples configurations from the *positive weight* ensemble

$$Z_k[\varphi] = \sum_{\{k_{x,\mu}\}} \rho[k;\varphi] = \sum_e Z_k^e \qquad Z_k^{e'}[\varphi] = \sum_{\{k_{x,\mu}\}} \rho[k;\varphi]\, \delta_{e[k],e'} \tag{2.33}$$

will be developed. The positive weight ensemble is connected to the original fermion ensemble by

$$Z_\xi^\epsilon = \sum_e Z_k^e\, \Phi[e,\epsilon] \qquad\qquad Z_k^e = \frac{1}{4}\sum_\epsilon Z_\xi^\epsilon\, \Phi[e,\epsilon]\ . \tag{2.34}$$

Expectation values obtained from the positive weight ensemble can be translated to expectation values obtained from the original fermion ensemble (2.3) by reweighting with $\Phi[e,\epsilon]$ (see appendix A for a summary of the different ensembles).

## 2.2 The global algorithm for free fermions

Following [17], a global algorithm sampling configurations from the positive weight ensemble $Z_k[\varphi]$ (2.33) is derived in two steps. After introducing bonds which freeze some of the dimers, new loops are constructed using a graphical method based on [18].

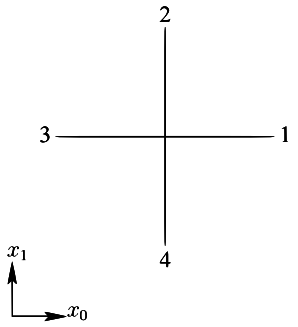


**Figure 2.3:** The dimers adjacent to $x$ are denoted by $1, 2, 3, 4$.

### 2.2.1 Bond variables

From the weight (2.31), a constraint $B[k]$ can be separated

$$\begin{aligned} \rho[k;\varphi] &= B[k] \cdot \tilde{\rho}[k;\varphi] \\ B[k] &= \begin{cases} 1 & \forall x \quad \sum\limits_{l, x\in\partial l} k_l = \text{even} \\ 0 & \text{else} \end{cases} \\ \tilde{\rho}[k;\varphi] &= \prod_x \tilde{f}_x(k,\varphi) \ . \end{aligned} \tag{2.35}$$

The dimer configuration weights $\tilde{\rho}$ must equal the weights $\rho$ for those configurations that have an even number[7] of dimers adjacent to each site. The weights $\tilde{f}_x$ can be completely expressed in terms of single, and of paired dimer variables at the site $x$. Again, for $B[k] = 1$ the $\tilde{f}_x$ have to coincide with the $f_x$. There are two ranges of $m$ or $\varphi$ respectively for which this is possible.

The directions of the dimers at $x$ will be denoted by 1 and 3 for forward and backward time direction, and with 2 and 4 for forward and backward space direction (see figure 2.3).

[7]Note that this also includes configurations with four dimers per site, which are forbidden by $\rho[k,\varphi] = 0$. The vanishing of the weights of these configurations has to be ensured by $\tilde{\rho}[k;\varphi] = 0$.

**Positive mass**

For positive mass, the local weights $\tilde{f}_x$ are

$$\begin{aligned}
\tilde{f}_x(k,\varphi) &= p\,[\delta_{k_1,0}+\delta_{k_2,0}+\delta_{k_3,0}+\delta_{k_4,0}] \\
&\quad + q\,[\delta_{k_1,0}\delta_{k_3,0}+\delta_{k_2,0}\delta_{k_4,0}] \\
&\quad + r\,[\delta_{k_1,0}\delta_{k_2,0}+\delta_{k_2,0}\delta_{k_3,0}+\delta_{k_3,0}\delta_{k_4,0}+\delta_{k_4,0}\delta_{k_1,0}] \\
r &= \frac{m(x)}{4} = \frac{\varphi(x)-2}{4} \\
p &= \frac{1}{2\sqrt{2}} - \frac{r}{2} = \frac{\sqrt{8}-m(x)}{8} \\
q &= 1 - \frac{1}{\sqrt{2}} + r = \frac{4-\sqrt{8}+m(x)}{4}\ .
\end{aligned} \tag{2.36}$$

The requirement that $p$, $q$ and $r$ can be interpreted as weights, and therefore have to be positive, yields

$$0 \le m(x) \le \sqrt{8} \approx 2.828\ . \tag{2.37}$$

**Negative mass**

With negative mass

$$\begin{aligned}
\tilde{f}_x(k,\varphi) &= \tilde{p}\,[\delta_{k_1,0}+\delta_{k_2,0}+\delta_{k_3,0}+\delta_{k_4,0}] \\
&\quad + \tilde{q}\,[\delta_{k_1,0}\delta_{k_3,0}+\delta_{k_2,0}\delta_{k_4,0}] \\
&\quad + \frac{\tilde{r}}{2}\,[\delta_{k_1,0}\delta_{k_2,1}+\delta_{k_2,0}\delta_{k_3,1}+\delta_{k_3,0}\delta_{k_4,1}+\delta_{k_4,0}\delta_{k_1,1} \\
&\qquad + \delta_{k_1,1}\delta_{k_2,0}+\delta_{k_2,1}\delta_{k_3,0}+\delta_{k_3,1}\delta_{k_4,0}+\delta_{k_4,1}\delta_{k_1,0}] \\
\tilde{r} &= -\frac{m(x)}{4} = \frac{2-\varphi(x)}{4} \\
\tilde{p} &= \frac{1}{2\sqrt{2}} - \frac{\tilde{r}}{2} = \frac{\sqrt{8}+m(x)}{8} \\
\tilde{q} &= 1 - \frac{1}{\sqrt{2}} - \tilde{r} = \frac{4-\sqrt{8}+m(x)}{4}\ ,
\end{aligned} \tag{2.38}$$

and now the $\tilde{p}$, $\tilde{q}$ and $\tilde{r}$ are all positive for

$$-1.172 \approx -4+\sqrt{8} \le m(x) \le 0\ . \tag{2.39}$$

The bounds (2.37) and (2.39) delimit the range of $m$ that can be treated with the algorithm.

**Bonds**

At this point, 10 or 14 bond variables[8] referring to the 10 or 14 (products of) Kronecker deltas in (2.36) and (2.38) are introduced and $\tilde{f}_x$ is rewritten to

$$\tilde{f}_x(k,\varphi) = \sum_i P_i \Delta_i(k_1,k_2,k_3,k_4;\varphi) \tag{2.40}$$

where the positive weights $P_i$ are the $\{p,q,r\}$ or $\{\tilde{p},\tilde{q},\tilde{r}\}$ corresponding to the 10 or 14 bonds $\Delta_i$, which represent the 10 or 14 Kronecker deltas in (2.36) or (2.38)[9]. The positive weight ensemble of dimer loops (2.33) can be expressed in terms of bonds and dimers

$$Z_k[\varphi] = \sum_{\{k_{x\mu}\},\{b_x\}} B[k] \prod_x P_{b_x} \Delta_{b_x}(k_1,k_2,k_3,k_4;\varphi) \ . \tag{2.41}$$

The bond configuration $\{b_x\}$ has to be *compatible* with the dimer configuration $\{k_{x,\mu}\}$ in order that their contribution to the partition function does not vanish.

An update in this ensemble may consist of two steps. First, for a given dimer configuration, the bonds are thrown in a heat bath sweep. Then, with some dimers frozen by the bonds, a new dimer configuration which is compatible with the bonds and with the constraint $B[k]$ is chosen.

The bonds are thrown in a heat bath sweep where the probability of throwing the bond $i$ is

$$\frac{\Delta_i P_i}{\sum_j \Delta_j P_j} \ . \tag{2.42}$$

For a valid configuration there is no site on which no bond is thrown. After freezing some of the dimers, a new dimer configuration can be constructed graphically.

### 2.2.2 Construction of new dimer loops for fixed bonds

First, it is noted that the weights $P_{b_x}$ originally stemming from the contribution of the dimers are now only used to pick a bond configuration. Consequently, for fixed bonds, all dimer configurations that are frozen by

[8]The concept of bond variables which are introduced by identically rewriting the weight of a configuration is in complete analogy to Swendsen-Wang [19] type algorithms (e.g., cluster algorithms for the Ising model [20]). The difference is that now there are more bond variables which have different weights while for the Ising model there is only one variable per link.

[9]For example, with $m > 0$, $\Delta_1 = \delta_{k_1,0}$ and $P_1 = p$. If the current configuration has $k_1 = 0$ at $x$, the bond which freezes $k_1$ to 0 will have the weight $P_1 = p$.

the bonds, and that obey the constraints $B[k] = 1$ (2.35) have to occur with the same probability. The task is to chose one of the possible dimer configurations completely at random.

The constraints can be treated as linear equations in the finite field $\{0, 1\}$ with an "addition" $\oplus$ defined by

$$1 \oplus 1 = 0 \oplus 0 = 0 \qquad 0 \oplus 1 = 1 \oplus 0 = 1 \ . \tag{2.43}$$

This "addition" resembles a logical `XOR`. In this formulation the requirement that there is an even number of dimers attached to each site (i.e., the requirement that $B[k] = 1$) is equivalent to

$$\forall x \bigoplus_{l, x \in \partial l} k_l = 0 \ . \tag{2.44}$$

The links where dimer variables are fixed by bonds form a set $\mathcal{B}$ and the constraint imposed by the bonds translates to[10]

$$k'_l = k_l \quad l \in \mathcal{B} \ . \tag{2.45}$$

A general solution of (2.44) and (2.45) can be constructed by "adding" one special solution of the whole inhomogeneous system ($k_l \neq 0$ in general) to the general solution of the inhomogeneous system

$$\begin{aligned} \bigoplus_{l, x \in \partial l} h_l = 0 \quad \forall x \\ h_l = 0 \quad l \in \mathcal{B} \ . \end{aligned} \tag{2.46}$$

As the constraints result from the previous configuration and hence have to be in accord with it, $\{k_l\}$ is a special solution of (2.44) and (2.45), and what remains to be done is to construct all general solutions $\{h_l\}$ of (2.46), pick one of them randomly and and take $\{k'_l\} = \{k_l \oplus h_l\}$ as the new configuration.

Having all $h_l$ with $l \in \mathcal{B}$ set to zero, $h_l = 1$ can only occur on links that belong to the complement of $\mathcal{B}$ denoted by $\bar{\mathcal{B}}$. Links belonging to $\bar{\mathcal{B}}$ will be called *predimers*. This name reflects the fact that it is the predimers from which the dimers of the general solution of the homogeneous system will eventually be made. From the fact that each $h_l$ has to fulfill two of the $V + |\mathcal{B}| = T \cdot L + |\mathcal{B}|$ equations[11] (2.46), it follows that closed non-intersecting and non-backtracking loops of predimers can be constructed. In a second step, the predimer loops will be discarded or kept to form dimer loops with 50% probability.

[10] Notation: Old dimer configuration $\{k\}$, new dimer configuration $\{k'\}$.

[11] $|A|$ denotes the cardinality of the set $A$.

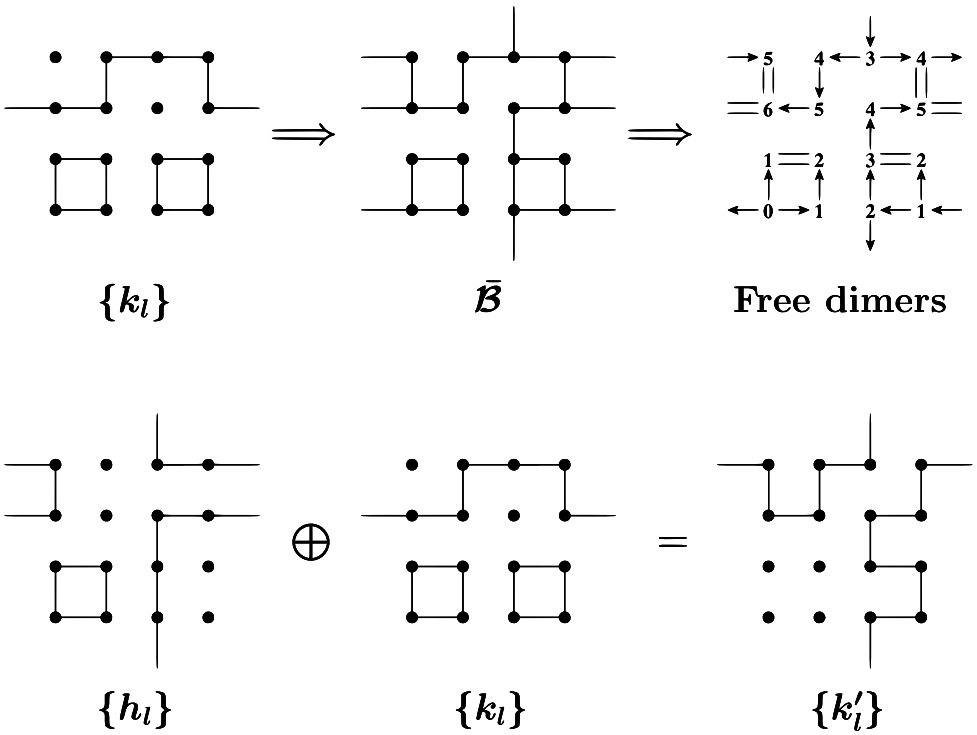


**Figure 2.4:** Construction of a new dimer configuration at frozen bonds. Starting with the dimer configuration $\{k_l\}$, bonds are thrown and the predimers (the links that are not fixed by a bond) $\bar{\mathcal{B}}$ result. Then, the spanning tree is constructed. (The arrows indicate the direction from which the site was added to the spanning tree. They are displayed to let the reader follow the construction. The numbers at the sites denote the level or distance from the root. The root is labeled 0. Free dimers are represented by two parallel lines.) In the next step the free dimers are deleted with probability 1/2 and the now unambiguous solution $\{h_l\}$ (of the homogeneous system) is constructed by solving $\bigoplus h_l = 0$ (only zero or two dimers survive) downwards level by level. This solution is "added" to the former configuration $\{k_l\}$ and produces the new configuration $\{k'_l\}$. The spanning tree and especially the location (not the number) of the free dimers depend on the very order in which the construction walks through the lattice. However, the configurations $\{h_l\}$ that are accessible do only depend on the predimers or on the bonds respectively.

To construct all solutions $\{h_l\}$ of (2.46), the technique of *spanning trees*, first used and proven in [18] and adapted to the loop gas algorithm in [17], is employed. Here, only the steps leading to a new configuration will be described. (For an illustrated example see figure 2.4). For a configuration $\{k_l\}$ the bonds $\mathcal{B}$ are thrown according to (2.42), and the predimers $\bar{\mathcal{B}}$ result. With the predimers fixed, the spanning tree and the special solution to the homogeneous system $\{h_l\}$ are found by repeating the following steps.

**Construction of the spanning trees and of new dimer loops**

- Walk through the lattice until a site, which (a) has at least one predimer attached, and (b) does not belong to any spanning tree, is met.

  Walk through the lattice until a site with at least one predimer that does not belong to any spanning tree is met. Name this site *root*. Construct the spanning tree:

  - Check whether the neighbors are connected by a predimer and if so, add them to the next level. *Levels* are integers which correspond to the distance from the root (measured along the spanning tree). The root belongs to level 0.
  - If the neighbor already already belongs to a level, the predimer connecting it to the current site is a *free dimer*.
  - Go to the next site of the current level, or, if all sites of the current level have already been considered, go to the next level. If no sites are left to consider, the construction of the spanning tree is finished.

- Delete the free dimers with probability 1/2. Free dimers that are not deleted become dimers which belong to the final $\{h_l\}$.[12]

- Go back to the root level by level and solve $\bigoplus h_l = 0$ at every site.[13]

- Walk on through the lattice and look for another root to start a new spanning tree from.

[12] This is where from all solutions of the homogeneous system one is picked randomly. All solutions $\{h_l\}$ of (2.46) are coded in the $2^{\#\text{free dimers}}$ possible choices of deleting or keeping free dimers.

[13] Since there are at most 3 predimers per site (the probabilities (2.42) do never vanish all), and since all dimers coming from higher levels are already fixed, the solution of $\bigoplus h_l = 0$ is always defined unambiguously.

With $\{h_l\}$, a new solution of the inhomogeneous system is

$$\{k'_l\} = \{k_l \oplus h_l\} \ . \tag{2.47}$$

## 2.3 The global algorithm for coupled flavors

First, the partition function for the interacting $N$ flavor Gross Neveu model is rewritten. Then, an effective contribution from a single flavor is separated from the partition function, and a valid update procedure that updates one flavor after another is discussed.

### 2.3.1 Coupling the flavors with the help of an $x$-dependent mass and a scalar field

By rendering the mass $x$-dependent, the quartic interaction can be written as[14] [1]

$$Z_{GN}^{\{z^i\}} = \exp\left[\frac{g^2}{2}\sum_x \frac{\partial^2}{\partial m(x)^2}\right] \prod_{i=1}^{N} Z_\xi^{z^i}[m]\Big|_{m(x)=m} \tag{2.48}$$

with the free single flavor partition function

$$Z_\xi^z[m] = \sum_\epsilon z(\epsilon) Z_\xi^\epsilon[m] \tag{2.49}$$

which contains the different boundary conditions according to their amplitudes $z(\epsilon)$. The exponential containing the derivative with respect to $m(x)$ can be expressed by a Gaussian integral

$$Z_{GN}^{\{z^i\}} = \int \mathrm{D}\sigma \, \exp\left[-\frac{1}{2}\sum_x \sigma^2(x) + g\sigma(x)\frac{\partial}{\partial m(x)}\right] \prod_{i=1}^{N} Z_\xi^{z^i}[m] \tag{2.50}$$

with the measure

$$\int \mathrm{D}\sigma \cdots \equiv \prod_x \int_{-\infty}^{\infty} \frac{\mathrm{d}\sigma(x)}{\sqrt{2\pi}} \cdots \ . \tag{2.51}$$

The term $g\sigma(x)\partial/\partial m(x)$ can be put into the free partition function. Then,

$$Z_{GN}^{\{z^i\}} = \int \prod_x \mathrm{d}\mu(\sigma(x)) \prod_{i=1}^{N} Z_\xi^{z^i}[m + g\sigma] \tag{2.52}$$

[14] The superscript $\{z^i\}$ denotes the set of distributions of the boundary conditions of all the flavors.

with the Gaussian measure

$$\int \mathrm{d}\mu(\sigma) = \int_{-\infty}^{\infty} \frac{\mathrm{d}\sigma(x)}{\sqrt{2\pi}} \, \mathrm{e}^{-\frac{1}{2}\sigma^2(x)} \ . \tag{2.53}$$

Since the $\xi$ are Grassmannian variables, only the first $N$ moments

$$\int \mathrm{d}\mu(\sigma)\sigma^n \ , \quad n = 0, \ldots, N \tag{2.54}$$

of the measure (2.53) contribute to the partition function (2.52), and every measure with the first $N$ moments identical to the Gaussian measure is valid. Later, it will be favorable to use a discrete distribution (see section 3.1).

### 2.3.2 Consequences for the algorithm and update procedure

Since the weight $\rho[k;\varphi]$ for each contribution factorizes into the contribution from the monomers (plus the auxiliary scalar field) and into the contribution from the dimers, the coupling of the flavors can be separated from the partition function

$$\prod_{i=1}^{N} \rho[k^i; \varphi + g\sigma] = \Big( \prod_{i=1}^{N} \rho[k^i; 1] \Big) \prod_x (\varphi + g\sigma)^{K(x)} \ . \tag{2.55}$$

The monomer number $K$ counts the number of flavors which have no dimers attached to the site $x$

$$K(x) = \sum_{i=1}^{N} \prod_{l, x \in \partial l} (1 - k_l^i) \ . \tag{2.56}$$

With (2.55), the $\sigma$-integration factorizes, and the partition function becomes

$$Z_{GN}^{\{z^i\}} = \sum_{\{k^i\}} \left[ \prod_{i=1}^{N} \rho[k^i; 1] \Phi[e^i; z^i] \right] \prod_x c(K(x), \varphi, g) \tag{2.57}$$

where the monomer contribution (and the coupling of the flavors) is contained in the factors

$$c(K(x), \varphi(x), g) = \int_{-\infty}^{\infty} \frac{\mathrm{d}\sigma(x)}{\sqrt{2\pi}} \mathrm{e}^{-\frac{\sigma^2}{2}} (\varphi(x) + g\sigma(x))^{K(x)} \ . \tag{2.58}$$

The sign $\Phi$ has been generalized to mixed boundary conditions

$$\Phi[e, z] = \sum_{\epsilon} z(\epsilon) \Phi[e, \epsilon] \ . \tag{2.59}$$

To derive an update procedure that changes only one flavor at a time, the monomer dependence of the weight $\rho$ must be restored for one single flavor:

$$\prod_{i=1}^{N} \rho[k^i;1] \prod_x c(K(x),\varphi(x),g) = \left\{ \prod_{i\neq j} \rho[k^i;1] \right\} \prod_x c(\tilde{K}^j(x),\varphi(x),g)\, \rho[k^j;\psi(\tilde{K}^j(x),\varphi(x),g)] \quad (2.60)$$

The reduced monomer number $\tilde{K}^j(x)$ counts the monomers in all flavors except for the flavor $j$

$$\tilde{K}^j(x) = K(x) - \delta_{K(x)|_j,1} \ . \quad (2.61)$$

The $\psi(\tilde{K}^j(x),\varphi(x),g)$ are the effective scalar fields $\varphi = 2+m$ seen by the flavor $j$ when the other flavors are fixed

$$\psi(K,\varphi,g) = \frac{c(K+1,\varphi,g)}{c(K,\varphi,g)} \ . \quad (2.62)$$

They obey the recursion

$$\psi(K,\ldots) = \varphi + \frac{g^2 K}{\psi(K-1,\ldots)} \qquad \psi(0,\ldots) = \varphi \ . \quad (2.63)$$

The fact that the effective single flavor weight $\rho[k^j;\psi,g]$ depends on $\psi$ and not directly on the fermion mass will have consequences for the range of parameters that is covered by the algorithm: While for the free case, the fermion mass $m$ has to obey the constraints (2.37) and (2.39) to render the weights $p,q$ and $r$ positive, the same constraints are now imposed on $\psi-2$ in the interacting case.

A valid update of the whole interacting system may employ the free fermion algorithm to update one flavor at a time, if the monomer contributions $\varphi(x)$ are replaced by $\psi(\tilde{K}^j(x),\varphi(x),g)$.

# Chapter 3

# Observables

The measurement of observables for the interacting theory is described. Then, the Green's functions are discussed, and the scalar correlation, which will be used to define the critical point, is introduced.

## 3.1 Observables for the interacting case

The ensemble $Z_{GN}^{\{z^i\}}$ (2.57) can be rewritten to the mixed form (dimers and auxiliary scalar field $\sigma(x)$)

$$Z_{GN,\sigma}^{\{z^i\}} = \int \prod_x \mathrm{d}\mu(\sigma(x)) \sum_{\{k^i\}} \left[\prod_{i=1}^{N} \rho[k^i;1]\Phi[e^i;z^i]\right] \prod_x \frac{(\varphi+g\sigma(x))^{K(x)}}{c(K(x))} c(K(x)) \ . \quad (3.1)$$

The corresponding positive weight ensemble is

$$Z_{\rho,\sigma} = \int \prod_x \mathrm{d}\mu(\sigma(x)) \sum_{\{k^i\}} \left[\prod_{i=1}^{N} \rho[k^i;1]\right] \prod_x \frac{(\varphi+g\sigma(x))^{K(x)}}{c(K(x))} c(K(x)) \ . \quad (3.2)$$

The expectation value $\langle \ldots \rangle_{\rho,\sigma}$ will refer to this ensemble. Then, the measurement $\langle A[\sigma] \rangle_{\rho,\sigma}$ can be translated to the positive weight ensemble $\langle \tilde{A}[K] \rangle_{\rho}$ with

$$\tilde{A}[K] = \int \prod_x \mathrm{d}\mu(\sigma(x)) A[\sigma(x)] \prod_x \frac{(\varphi+g\sigma(x))^{K(x)}}{c(K(x))} \ . \quad (3.3)$$

Further translation to the full Gross Neveu ensemble then can be achieved by reweighting (see appendix A.3). The sign of each $N$ flavor configuration then is the product of the $\Phi[e^i, z^i]$ for each flavor.

If the integration in (3.3) cannot be done analytically, a stochastic integration which for every site $x$ picks a $\sigma$ from the distribution

$$P(\sigma)\mathrm{d}\sigma \propto (\varphi + g\sigma)^K \mathrm{d}\mu(\sigma) \tag{3.4}$$

can be used to evaluate the integral.

Numerically it is more convenient not to use the full Gaussian measure (2.53) to pick the $\sigma$'s. There are weights $w_i$ and values $\sigma_i$ for which the first $N$ moments of the continuous measure (2.53) coincide with those of the discrete distribution $(w_i, \sigma_i)$:

$$\int \mathrm{d}\mu(\sigma)\sigma^K = \sum_{i=1}^{n} w_i(\sigma_i)^K \quad \text{for } K = 0, 1, \ldots, N \ . \tag{3.5}$$

These weights turn out to be the weights used for the Gauss-Hermite integration method [21]. To obtain the desired distribution (3.4), the weights $w_i$ have to be replaced by

$$w_i \to \tilde{w}_i(K) = \frac{w_i \cdot (\varphi + g\sigma_i)^K}{\sum_j w_j \cdot (\varphi + g\sigma_j)^K} \ . \tag{3.6}$$

Due to the fact that the $\tilde{w}_i(K)$ are the weights proportional to which the $\sigma_i$ will be picked, they must not be negative. The requirement of positivity of the $\tilde{w}_i(K)$ will lead to another constraint to the range of $(m, g^2)$ covered by the algorithm. As discussed in section 7.1, this constraint will be the first to be met, when the coupling constant $g^2$ is increased.

## 3.2 Solving for the Green's function

### 3.2.1 The Wilson Dirac operator and the Green's function

The free Wilson Dirac operator is

$$\begin{aligned} D &= \tilde{\partial\!\!\!/} - \frac{1}{2}\partial\partial^* + m \\ D_{x,y;a,b} &= (m+2)\,\delta^{(2)}_{x,y}\,\delta_{a,b} - \beta_{+\mu}(x)\,\delta^{(2)}_{x,y-\hat{\mu}}\,P_{a,b}(\hat{\mu}) \\ &\quad + \beta_{-\mu}(x)\,\delta^{(2)}_{x,y+\hat{\mu}}\,P_{a,b}(-\hat{\mu}) \ . \end{aligned} \tag{3.7}$$

The lattice size is $L_0 = T$ for the time direction and $L_1 = L$ for the space direction. The second line represents the full spinor $(a, b)$ and position space

$(x, y)$ index structure with the Wilson projectors $P(\hat{\mu})$. The boundary conditions $\epsilon$ are taken into account by

$$\begin{aligned} \beta_{+\mu}(x) &= \begin{cases} (-1)^{\epsilon_\mu} & \text{if } x_\mu = L_\mu - 1, \\ +1 & \text{else ,} \end{cases} \\ \beta_{-\mu}(x) &= \begin{cases} (-1)^{\epsilon_\mu} & \text{if } x_\mu = 0, \\ +1 & \text{else .} \end{cases} \end{aligned} \tag{3.8}$$

The Green's function $G$ is defined by

$$\begin{aligned} D\,G &= \mathbf{1} \\ D_{x,y;a,b}\,G_{y,z;b,c} &= \delta^{(2)}_{x,z}\,\delta_{a,c}\ . \end{aligned} \tag{3.9}$$

Solving (3.9) amounts to the inversion of a $2TL \times 2TL$ matrix representing the Wilson Dirac operator $D$.

### 3.2.2 Indices and periodicity

The index structure of the Wilson Dirac operator $D$, and of the Green's function $G$ can be mapped to a single index

$$n_{x;a} = n_{x_0,x_1;a} = x_0 + T \cdot x_1 + TL \cdot a\ . \tag{3.10}$$

In order to respect the toroidal periodicity of the lattice, an addition of two vector components has to be mapped back to $0, \ldots, L_\mu - 1$ by

$$n_{x+y;a} = n_{(x_0+y_0)\mathrm{mod}T,(x_1+y_1)\mathrm{mod}L;a}\ . \tag{3.11}$$

The same is true for the Kronecker deltas $\delta^{(2)}_{x,y}$ which have to be understood as

$$\delta^{(2)}_{x,y} = \delta_{x_0,y_0} \cdot \delta_{x_1,y_1} = \delta_{(x_0-y_0)\mathrm{mod}T,0} \cdot \delta_{(x_1-y_1)\mathrm{mod}L,0}\ . \tag{3.12}$$

### 3.2.3 Inverting the Wilson Dirac operator

In this work, the relation (3.9) was not directly inverted. Instead, the fact that $(\mathcal{C}D)^2$ is a negative definite matrix was used, and the Green's function was obtained by solving

$$(\mathcal{C}D)^2 G = \mathcal{C}D\mathcal{C}\mathbf{1} \tag{3.13}$$

iteratively using a conjugate gradient method.

### 3.2.4 The scalar correlation

The fermion two point function in the Gross Neveu ensemble with boundary conditions distributed according to the amplitudes $z^i(\epsilon)$

$$\left\langle \xi^a(x)\xi^{aT}(y)\mathcal{C}\right\rangle_{GN}^{\{z^i\}} = \frac{\left\langle \overline{G}^{z^a}(x,y;g\sigma;e^a)\prod_i \Phi[e^i;z^i]\right\rangle_{\rho,\sigma}}{\left\langle \prod_i \Phi[e^i;z^i]\right\rangle_{\rho}} \tag{3.14}$$

will be considered[1]. $\overline{G}^{z^a}$ is the averaged Green's function

$$\overline{G}^{z^a}(x,y;g\sigma;e^a) = \frac{1}{\Phi[e^a,z^a]}\sum_{\epsilon}\Phi[e^a,\epsilon]z^a(\epsilon)G(x,y;g\sigma;\epsilon) \tag{3.15}$$

where the Green's function $G(x,y;g\sigma;\epsilon)$ is the inverse of the Dirac operator with boundary conditions $\epsilon$, and with the mass $m(x)+g\sigma(x)$ on the diagonal.

Choosing the distribution of the boundary conditions to

$$\bar{z}(\epsilon) = 1/2 - \delta_{\epsilon,0} \tag{3.16}$$

renders the sign $\Phi$ trivial

$$\Phi[e;\bar{z}] = 1 \quad \forall e\ . \tag{3.17}$$

The averaged Green's function becomes

$$\overline{G}^{\bar{z}}(x,y;g\sigma;e^a) = \sum_{\epsilon}(1/2 - \delta_{e_0,\epsilon_1}\delta_{e_1,\epsilon_0})G(x,y;g\sigma;\epsilon)\ , \tag{3.18}$$

and the two point function simplifies to

$$\left\langle \xi^a(x)\xi^{aT}(y)\mathcal{C}\right\rangle_{GN}^{\{\bar{z}\}} = \left\langle \sum_{\epsilon}(1/2 - \delta_{e_0,\epsilon_1}\delta_{e_1,\epsilon_0})G(x,y;g\sigma;\epsilon)\right\rangle_{\rho,\sigma}\ . \tag{3.19}$$

The two point function is projected to the spatially periodic contributions[2] by summing over $2L$ successive values in the time slices belonging to $x_0$, and to $y_0$. With the definitions

$$\breve{\xi}(x_0) = \sum_{x_1=0}^{2L}\xi(x0,x1) \quad \breve{G}(x_0,y_0,g\sigma,\epsilon) = \frac{1}{2L}\sum_{x_1,y_1=0}^{2L}G(x,y;g\sigma;\epsilon)\ , \tag{3.20}$$

the time slice correlation function emerges

$$\begin{aligned}\frac{1}{2L}\left\langle \breve{\xi}^a(x_0)\breve{\xi}^{aT}(0)\mathcal{C}\right\rangle_{GN}^{\{\bar{z}\}} &= \left\langle (1/2 - \delta_{e,(00)})\breve{G}(x_0,0;g\sigma;(00))\right\rangle_{\rho,\sigma} \\ &\quad + \left\langle (1/2 - \delta_{e,(01)})\breve{G}(x_0,0;g\sigma;(10))\right\rangle_{\rho,\sigma}\ .\end{aligned} \tag{3.21}$$

[1] The flavor index $a$ is not summed!

[2] Note that due to the mixed boundary conditions distributed with $z(\epsilon)$, the fields $\xi$ are neither periodic, nor anti-periodic.

Defining the scalar time slice correlation as the trace[3] of the time slice correlation

$$k_S(x_0) = \frac{1}{2L} \operatorname{tr} \left\langle \breve{\xi}^a(x_0) \breve{\xi}^{aT}(0) \mathcal{C} \right\rangle_{GN}^{\{\bar{z}\}} , \tag{3.22}$$

and projecting on the temporally anti-periodic contribution

$$\tilde{k}_S(x_0) = \frac{1}{2} \Big[ k_S(x_0) - k_S(x_0 + T) \Big] \tag{3.23}$$

yields

$$\tilde{k}_S(x_0) = \Big\langle (1/2 - \delta_{e,(01)}) \operatorname{tr} \Big[ \breve{G}(x_0, 0; g\sigma; (10)) \Big] \Big\rangle_{\rho,\sigma} . \tag{3.24}$$

In chapter 5, $\tilde{k}_S(T/4)$ will be used to define the critical point.

## 3.3 Variables which are directly used by the loop gas algorithm

In contrast to the Green's function which needs an (expensive) inversion of a large matrix, there are variables which are directly used by the loop gas algorithm and hence can be measured with negligible effort.

In the next chapter, the monomer number $K(x)$ and the time slice correlation of the monomer number will be measured. It will be shown to be related to the zero distance correlation of the fermion fields.

In chapter 5, the order parameter $\chi$ which can be mapped to expectation values of the topology of the dimer configurations of the interacting theory, will be introduced. As the topologies of the different flavors can be easily tracked during the update process, this order parameter will turn out to be a very cheap observable (with respect to computer time needed for a desired precision).

[3]The trace is computed with respect to spinor indices.

# Chapter 4

# Testing the algorithm for free fermions

The fact that the free propagator is known analytically is employed to test the algorithm. The monomer number, and the two point correlation of the monomer number are measured with high precision. The sensitivity of the algorithm to the choice of the random numbers is examined.

## 4.1 Monomer number and two point function for free fermions

### 4.1.1 Analytic results

The expectation value for the monomer number

$$\frac{\langle K(x)\Phi\rangle_\rho}{\langle\Phi\rangle_\rho} = -\frac{\varphi(x)}{2}\,\langle\xi^T(x)\mathcal{C}\xi(x)\rangle_\xi^\epsilon \tag{4.1}$$

is proportional to the (spinor index) trace of the zero distance propagator (see section 1.2.2)

$$\frac{\langle K(x)\Phi\rangle_\rho}{\langle\Phi\rangle_\rho} = \frac{m+2}{2}\,\mathrm{tr}[G(0)] = \frac{m+2}{TL}\sum_p \frac{M}{\mathring{p}^2+M^2}\ . \tag{4.2}$$

For vanishing mass $m$ and for boundary conditions that are periodic in time and in space this expectation value must diverge. On the left hand side the divergence is realized by cancelling fluctuations of the sign $\Phi$.

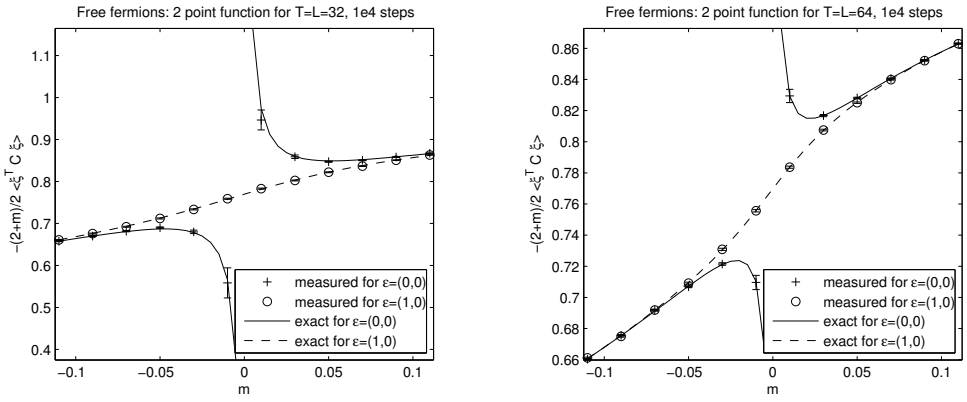


(a) $T = L = 32$ (b) $T = L = 64$

**Figure 4.1:** Two point function for $m = -0.11 \ldots + 0.11$. Boundary conditions are $\epsilon = (0, 0)$ and $\epsilon = (1, 0)$. All measurements accord with the theoretical value within the errors. The data for each point were obtained from $10^4$ updates after $10^3$ thermalization steps.

### 4.1.2 Measurements

The monomer density was measured for different lattice sizes close to the critical mass $m = 0$. Then, it was reweighted to yield the zero distance propagator with the boundary conditions $\epsilon$. The results for $T = L = 32, 64$, $m = -0.11 \ldots 0.11$, and $\epsilon = (0, 0), (1, 0)$ are displayed in figure 4.1. For the other boundary conditions the deviations from the case $\epsilon = (1, 0)$ are very small.

Table 4.1 displays some measurements and theoretical values for $T = L = 32, 64$. The Monte Carlo and the theoretical values differ by up to $1.4\sigma$.

## 4.2 Testing the sensitivity to the choice of the random number generator

In order to make sure that the loop gas algorithm is not sensitive to the random number generator (rng) that is used in the Monte Carlo step, tests with different Generators have been performed. Four different rng's that are available in the *GNU Scientific Library*[1] have been used:

- **taus:** A maximally equidistributed combined Tausworthe generator [22],

[1]GSL – GNU Scientific Library: `http://www.gnu.org/software/gsl/`, visited 2008-09-16.

| $T = L$ | $m$ | $K_{theo}$ | $K_{MC}$ |
|---|---|---|---|
| | | $\epsilon = (0,0)$ | |
| 32 | $-0.11$ | 0.65770 | 0.6577(11) |
| 32 | $+0.11$ | 0.86655 | 0.86722(67) |
| 64 | $-0.11$ | 0.66056 | 0.66031(50) |
| 64 | $+0.11$ | 0.86287 | 0.86310(30) |
| | | $\epsilon = (0,1)$ | |
| 32 | $-0.11$ | 0.66099 | 0.6594(11) |
| 32 | $+0.11$ | 0.86224 | 0.86278(64) |
| 64 | $-0.11$ | 0.66060 | 0.66034(49) |
| 64 | $+0.11$ | 0.86279 | 0.86296(31) |
| | | $\epsilon = (1,0)$ | |
| 32 | $-0.11$ | 0.66099 | 0.6608(11) |
| 32 | $+0.11$ | 0.86224 | 0.86313(68) |
| 64 | $-0.11$ | 0.66060 | 0.66112(53) |
| 64 | $+0.11$ | 0.86279 | 0.86296(30) |
| | | $\epsilon = (1,1)$ | |
| 32 | $-0.11$ | 0.66256 | 0.6626(11) |
| 32 | $+0.11$ | 0.86045 | 0.86109(66) |
| 64 | $-0.11$ | 0.66064 | 0.66046(53) |
| 64 | $+0.11$ | 0.86272 | 0.86282(30) |

**Table 4.1:** Zero distance propagator $K = -\varphi(x)/2 \left\langle \xi^T(x)\mathcal{C}\xi(x)\right\rangle_\xi^\epsilon$ measured at different masses and for $T = L = 32, 64$. The measurements and the theoretical values differ by up to $1.4\sigma$.

- **twister:** a Mersenne Twister based algorithm [23],
- **ranlxd2:** a *luxury level 2* double precision version of the RANLUX generator [24, 25],
- **rand48:** the UNIX rand48 generator.

All four generators produced results that were in agreement with the theoretical values up to $0.07 \ldots 1.47\sigma$ (see table 4.2). For the rest of the work the fastest generator **taus** was used, because it reduced the computer time used for a complete simulation by up to 35% compared to **ranlxd2**.

## 4.3 Correlations of the monomer number for free fermions

### 4.3.1 Analytic results

Using $\varphi(y)\partial/\partial\varphi(y)$ on (4.1) again (for $x \neq y$) results in

$$\frac{4}{(m+2)^2}\left[\frac{\langle K(y)K(x)\Phi\rangle_\rho}{\langle\Phi\rangle_\rho} - \frac{\langle K\Phi\rangle_\rho^2}{\langle\Phi\rangle_\rho^2}\right] = \langle\xi^T(y)\mathcal{C}\xi(y)\xi^T(x)\mathcal{C}\xi(x)\rangle_\xi^\epsilon - \langle\xi^T(y)\mathcal{C}\xi(y)\rangle_\xi^\epsilon \langle\xi^T(x)\mathcal{C}\xi(x)\rangle_\xi^\epsilon \ . \tag{4.3}$$

The left hand sides coincide (compare (4.1))

$$\frac{4}{(m+2)^2}\frac{\langle K(y)K(x)\Phi\rangle_\rho}{\langle\Phi\rangle_\rho} = \langle\xi^T(y)\mathcal{C}\xi(y)\xi^T(x)\mathcal{C}\xi(x)\rangle_\xi^\epsilon \ . \tag{4.4}$$

Application of Wick's theorem yields

$$\frac{4}{(m+2)^2}\frac{\langle K(y)K(x)\Phi\rangle_\rho}{\langle\Phi\rangle_\rho} = \mathrm{tr}[G(0)]^2 - 2\,\mathrm{tr}[G(y-x)G(x-y)] \ . \tag{4.5}$$

With the time averaged monomer density defined by

$$k(t) = \frac{1}{L}\sum_{x_1} K(t, x_1), \tag{4.6}$$

the time slice correlation function of the monomer density is (for $t \neq 0$)

$$\frac{4}{(m+2)^2}\frac{\langle k(t)k(0)\Phi\rangle_\rho}{\langle\Phi\rangle_\rho} = \mathrm{tr}[G(0)]^2 - \frac{2}{L}\sum_{y_1}\mathrm{tr}[G(t,y_1)G(-t,-y_1)] \ . \tag{4.7}$$

This expression can be evaluated numerically.

| **RNG** | **taus** | **twister** | **ranlxd2** | **rand48** |
|---|---|---|---|---|
| | 0.953265(86) | 0.953252(87) | 0.953334(88) | 0.953241(89) |
| | 0.953326(87) | 0.953348(87) | 0.953201(89) | 0.953249(88) |
| | 0.953218(87) | 0.953325(89) | 0.953147(89) | 0.953333(86) |
| | 0.953447(88) | 0.953200(88) | 0.953249(88) | 0.953413(88) |
| | 0.953260(88) | 0.953122(88) | 0.953285(89) | 0.953180(87) |
| | 0.953313(87) | 0.953129(87) | 0.953100(89) | 0.953369(87) |
| | 0.953423(88) | 0.953366(87) | 0.953164(88) | 0.953174(89) |
| | 0.953273(87) | 0.953149(88) | 0.953279(88) | 0.953384(88) |
| | 0.953171(88) | 0.953202(88) | 0.953184(90) | 0.953239(89) |
| $\frac{\langle K\Phi\rangle_\rho}{\langle\Phi\rangle_\rho}$ | 0.953335(86) | 0.953358(87) | 0.953337(88) | 0.953338(87) |
| | 0.953241(86) | 0.953120(88) | 0.953288(88) | 0.953163(88) |
| | 0.953170(88) | 0.953221(89) | 0.953284(87) | 0.953294(87) |
| | 0.953137(86) | 0.953379(87) | 0.953247(88) | 0.953311(89) |
| | 0.953235(86) | 0.953398(87) | 0.953240(88) | 0.953449(87) |
| | 0.953294(88) | 0.953311(88) | 0.953255(88) | 0.953361(89) |
| | 0.953180(87) | 0.953174(87) | 0.953361(88) | 0.953233(88) |
| | 0.953352(87) | 0.953311(88) | 0.953299(88) | 0.953151(88) |
| | 0.953229(88) | 0.953251(89) | 0.953340(86) | 0.953257(89) |
| | 0.953159(90) | 0.953187(88) | 0.953315(89) | 0.953417(87) |
| | 0.953266(88) | 0.953344(87) | 0.953283(88) | 0.953242(87) |
| **mean** | 0.953265(20) | 0.953258(20) | 0.953260(20) | 0.953291(20) |
| **theory** | 0.9532617 | | | |
| **dev.** | $0.16\sigma$ | $-0.20\sigma$ | $-0.07\sigma$ | $1.47\sigma$ |

**Table 4.2:** Testing the random number generator: Measurements of $\langle K\Phi\rangle_\rho / \langle\Phi\rangle_\rho$ for $\epsilon = (1, 0)$, $m = 0.5$, and $T = L = 32$. 20 runs averaged and compared to the theoretical value. The deviations from the theoretical value show no large discrepancies, and the single runs do not show any systematic underestimations or overestimations. Warning: The small deviation produced with **ranlxd2** and the large deviation produced with **rand48** are mere coincidence and should not be over-interpreted. Rerunning the test with a different set of seeds and different numbers of runs per generator yields fluctuations of the deviation from $-2\sigma$ to $+2\sigma$ for all four generators. Altogether, the loop gas algorithm was not found to be sensitive to the random number generator.

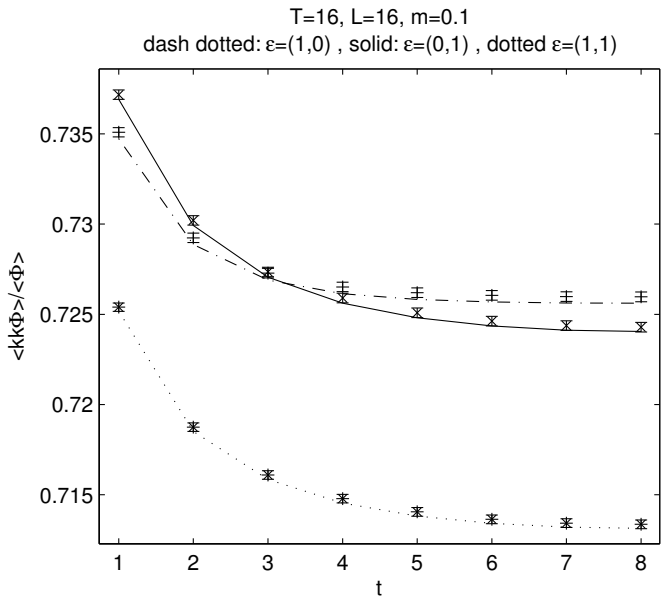


**Figure 4.2:** Time slice correlation of the monomer density determined according to (4.7). The boundary conditions $\epsilon = (1, 0)$ (dash dotted line), $\epsilon = (0, 1)$ (solid line) and $\epsilon = (1, 1)$ (dotted line) are plotted. The lines represent the analytical result obtained from evaluation of (4.7). The measurements were done using $10^6$ steps after $10^5$ thermalization steps.

### 4.3.2 Measurements

The time slice correlation of the monomer density has been measured on a lattice of the size $16 \times 16$ and for a mass $m = 0.1$. In figure 4.1, the results for different boundary conditions are plotted together with the theoretical values. They agree within $0.5 \ldots 1.1\sigma$.

The algorithm has passed the test for the free case. In the next chapter it will be used to simulate the interacting theory. Two different observables will be used to tune the mass to its critical value.

# Chapter 5

# Tuning the mass

Two different observables are used to define the critical mass $m_c$ which for given coupling $g^2$ restores the chiral symmetry in the continuum limit. The first definition uses the topology of the dimer configurations, and the second definition uses the scalar correlation. The two definitions of the critical mass are compared in the infinite volume limit. Then, the critical line $m_c(g^2)$ is determined and compared to the leading order perturbation theory prediction.

## 5.1 Order parameters

### 5.1.1 The order parameter $\chi$

In [26], it is argued, that the free single flavor partition function $Z_\xi^\epsilon$ vanishes at the critical point if the boundary conditions are periodic in both directions ($\epsilon = 0$), and that $Z_\xi^\epsilon$ does not vanish if there is at least one direction with anti-periodic boundary conditions ($\epsilon \neq 0$). Using (2.33), it can be shown that the original fermion partition function $Z_\xi^\epsilon$ with boundary conditions $\epsilon$ can be "measured" in the positive weight ensemble $Z_k$ as

$$Z_\xi^{00} = -Z_k \left\langle 1 - 2\delta_{e,0} \right\rangle_k \ . \tag{5.1}$$

Furthermore, the sum of the partition functions which do not vanish at the critical point ($\epsilon \neq 0$) is

$$Z_\xi^{01} + Z_\xi^{10} + Z_\xi^{11} = Z_k \left\langle 1 + 2\delta_{e,0} \right\rangle_k \ . \tag{5.2}$$

As the free $N$ flavor partition function factorizes into the contributions from the flavors, the critical point for (still free) $N$ flavors can be defined by the

vanishing of

$$\sum_{j=1}^{N} \langle 1 - 2\delta_{e^j,0} \rangle_{k^j} \prod_{i \neq j} \langle 1 + 2\delta_{e^i,0} \rangle_{k^i} = \sum_{j=1}^{N} \left\langle (1 - 2\delta_{e^j,0}) \prod_{i \neq j} (1 + 2\delta_{e^i,0}) \right\rangle_{\{k\}} \tag{5.3}$$

Generalization of this idea to the interacting theory yields the order parameter

$$\chi = \frac{1}{N} \sum_{j=1}^{N} \left\langle (\delta_{e^j,0} - 1/2) \prod_{i \neq j} (1/2 + \delta_{e^i,0}) \right\rangle_{\rho} . \tag{5.4}$$

As the topology of the dimer configurations can be easily tracked during the update process, $\chi$ can be measured with almost no additional computer time.

### 5.1.2 Using the Green's function: $k_S(T/4)$

As discussed in section 1.2.3, the critical mass can also be defined by the vanishing of the scalar correlation. Here, the scalar time slice correlation

$$\tilde{k}_S(x_0) = \left\langle (1/2 - \delta_{e,(01)}) \operatorname{tr}\left[ \breve{G}(x_0, 0; g\sigma; (10)) \right] \right\rangle_{\rho,\sigma} . \tag{5.5}$$

defined in section 3.2.4 will be used. As in [14], where a similar quantity was used to define the chiral point, the critical mass will be defined as that mass for which $\tilde{k}_S(T/4)$ vanishes.

## 5.2 Tuning procedure – Example: $N = 6$, $T = L = 16$, $g^2 = 0.2$

The critical mass, defined as the value of the mass parameter at which the order parameter vanishes, will be determined by finding the sign change in the order parameter. For the order parameters $\chi$ and $k_S(T/4)$, a typical $m$ dependence is displayed in figure 5.1. Compared to those for $m > m_c$, the values of $\chi$ for $m < m_c$ are very close to zero. However, with enough statistics $\chi(m < m_c)$ is always significantly negative and it is possible to find a sign change at $m = m_c$. The sign change of the order parameter $k_S(T/4)$ is much more pronounced than the sign change of $\chi$.

The procedure of finding the critical mass is the following. First, a mixture of the bisection and the secant method is employed to pin down the

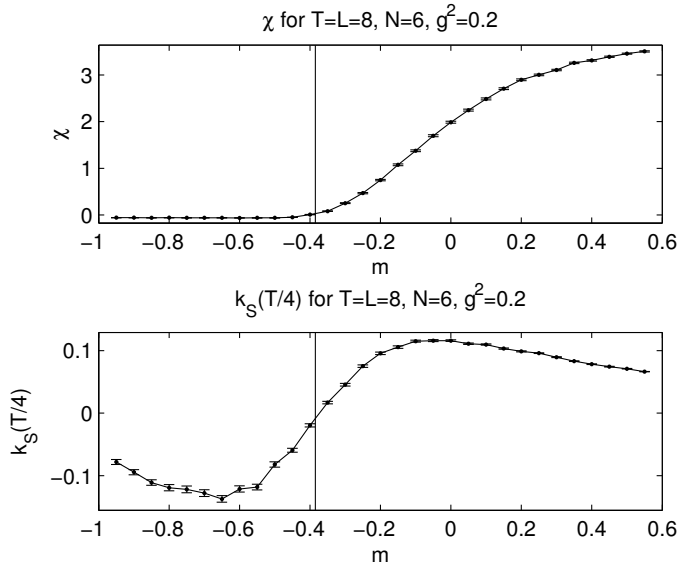


**Figure 5.1:** $N = 6$, $T = L = 8$, $g^2 = 0.2$: $\chi$ and $k_S(T/4)$ for $m = -0.95 \ldots 0.55$. The sign changes are near $m = -0.38$ (marked by the vertical line). Note that for $m < -0.38$, $\chi$ is very close to zero (but with enough statistics always significantly negative).

region which contains the sign change in $\chi(m)$ to at least $\pm 4\sigma$ (using a fixed number of MC steps per value of $m$). Then, in this region, the order parameter $\chi$ is measured for five different masses. Finally, the five measurements are linearly and quadratically interpolated to $m(\chi = 0)$. The critical mass is estimated from the linear fit. The error is assumed to consist of two parts: A statistical error determined by error propagation of the linear fit results, and a systematic error estimated from the discrepancy between the linear and the quadratic fit results.

As an example, the tuning is described for $T = L = 16$, $N = 6$, and $g^2 = 0.2$. The order parameter is $\chi$. Figure 5.2 shows the five measurements used

| $m_0$ | $\chi$ |
|---|---|
| $-0.39531250$ | $-0.00335(15)$ |
| $-0.39476859$ | $-0.00120(15)$ |
| $-0.39422468$ | $+0.00032(16)$ |
| $-0.39398734$ | $+0.00100(16)$ |
| $-0.39375000$ | $+0.00170(16)$ |

**Table 5.1:** $T = L = 16$, $N = 6$, $g^2 = 0.2$: Order parameter $\chi$ for $2 \cdot 10^6$ steps after $2 \cdot 10^5$ thermalization steps.

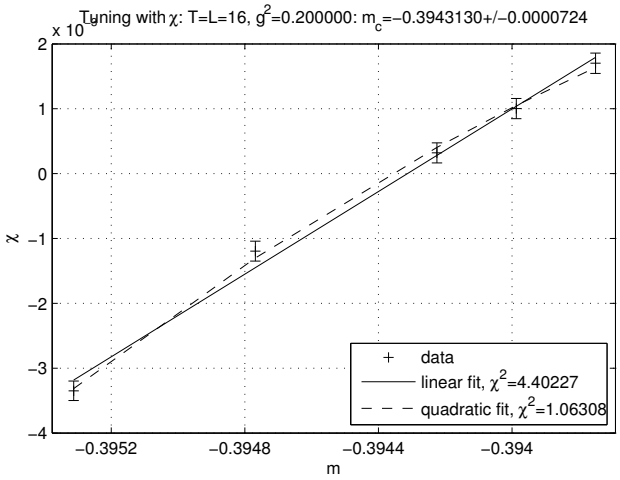


**Figure 5.2:** $T = L = 16$, $N = 6$, $g^2 = 0.2$: Order parameter $\chi$ for $2 \cdot 10^6$ steps after $2 \cdot 10^5$ thermalization steps. The critical mass is determined by fitting $\chi(m)$ linearly. The statistical error is determined by error propagation of the linear fit results. The systematic error is determined from the discrepancy between the linear fit results and the quadratic fit results. The critical mass is $m_c = -0.394313(22 + 50)$ (with error = statistical + systematic).

in the interpolation. $2 \cdot 10^6$ steps are used to measure $\chi$ per value of $m$. The data are displayed in table 5.1. The result (error = statistical + systematic) is

$$\mathbf{m_c = -0.394313(22 + 50)} \ . \tag{5.6}$$

## 5.3 Comparison of tuning with $\chi$ and with $k_S(T/4)$

The two order parameters $\chi$ and $k_S(T/4)$ described in section 5.1 will be used to tune the mass for different numbers of flavors $N = 2, 4, 6$, for coupling constants $g^2 = 1/(N-1)$, and for a sequence of lattice sizes $T = L = 4, 8, 16, 32, 64$. Then, linear extrapolations to $T = L \to \infty$ will be made for both, the masses tuned with $\chi$, and the masses tuned with $k_S(T/4)$. In the infinite volume limit, the critical masses obtained with $\chi$ and with $k_S(T/4)$ are found to be compatible.

The parameters have been chosen in order to simulate in the unbroken phase (see section 6.2) without violating any of the constraints summarized in section 7.1. For example, the coupling constants are chosen such that leading order perturbation theory predicts a critical mass close to $m = -0.4$ which is far from the lower bound $-1.17 < m$.

| | $N$ | $m_c^\infty$ | $\alpha$ | $\chi^2$ |
|---|---|---|---|---|
| $\chi$ | 2 | $-0.46310(59)$ | 0.0055(70) | 0.6 |
| $k_S(T/4)$ | 2 | $-0.46410(58)$ | 0.205(21) | 1.1 |
| $\chi$ | 4 | $-0.40149(14)$ | 0.0017(53) | 2.6 |
| $k_S(T/4)$ | 4 | $-0.40161(11)$ | 0.1583(45) | 5.9 |
| $\chi$ | 6 | $-0.39442(16)$ | 0.0042(61) | 1.6 |
| $k_S(T/4)$ | 6 | $-0.394492(86)$ | 0.1545(28) | 3.9 |

**Table 5.2:** $m_c^\infty + \alpha/T$ fitted to the critical mass tuned with $\chi$ or with $k_S(T/4)$. For each $N$, the limits $m_c(T \to \infty)$ agree. For $N = 2$ and $k_S(T/4)$, and for $N = 6$ and $\chi$ the fits were done without the $T = L = 4$ data. For the tuning with $\chi$ the linear corrections $\alpha$ vanish.

The results for $N = 2, 4$, and $N = 6$ flavors are plotted in figures 5.3 to 5.5. Fitting the $T$-dependence of the critical mass with

$$m_c = m_c^\infty + \frac{\alpha}{T} + O\left(\frac{1}{T^2}\right) \tag{5.7}$$

yields the results displayed in table 5.2. The infinite volume limits $m_c^\infty$ obtained with linear extrapolation of the $\chi$ and $k_S(T/4)$ tuned masses are all compatible within the errors.

The parameter $\chi$ is more efficient for tuning the critical mass, because (a) the evaluation of $\chi$ needs much less computer time[1], and (b) the coefficient $\alpha$ which determines the size of $O(T^{-1})$ corrections to $m_c$ vanishes for tuning with $\chi$.

## 5.4 Critical line for $N = 6$

The critical line $m_c(g^2)$ was determined for $N = 6$ flavors, and for different lattice sizes $T = L = 4, 8, 16, 32$. As the range of $m$ that can be treated with the algorithm is limited by (see (2.37) and (2.39))

$$-1.172 \approx -4 + \sqrt{8} \le m \le \sqrt{8} \approx 2.828 \ , \tag{5.8}$$

the range of the coupling for which $m_c$ can be estimated is limited to $g^2 = 0, \ldots, 0.55$.

The procedure described in section 5.2 was repeated for $g^2 = 0, \ldots, 0.55$ and $T = L = 4, 8, 16, 32$. The data for $\chi(m)$ and the resulting $m_c$ are compiled in appendix B. The critical line $m_c(g^2)$ for $T = L = 4, 8, 16, 32$ is

[1] See section 7.3 on convergence of the solver.

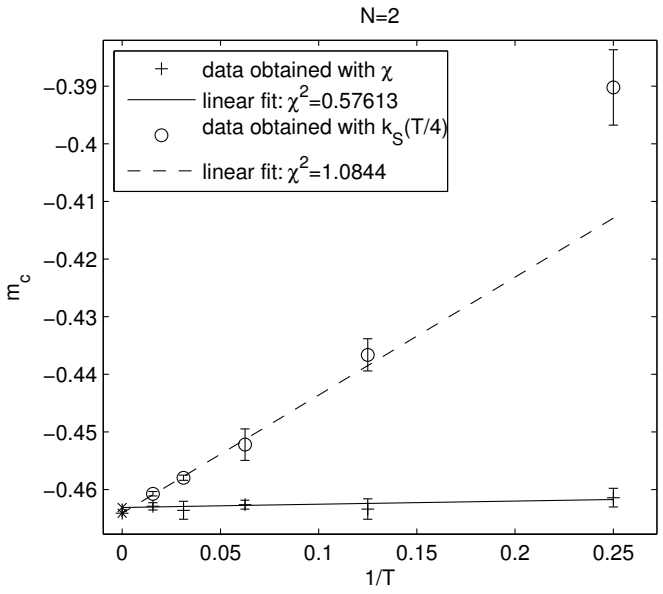


**Figure 5.3:** Critical mass for $T = L = 4, 8, 16, 32, 64$, $N = 2$ and $g^2 = 1$. Tuned with $\chi$ and with $k_S(T/4)$. The results of the linear fits are $m_c^{\chi}(T \to \infty) = -0.46310(59)$ and $m_c^{k}(T \to \infty) = -0.46410(58)$. The fit for $k_S(T/4)$ was done without the $T = L = 4$ data.

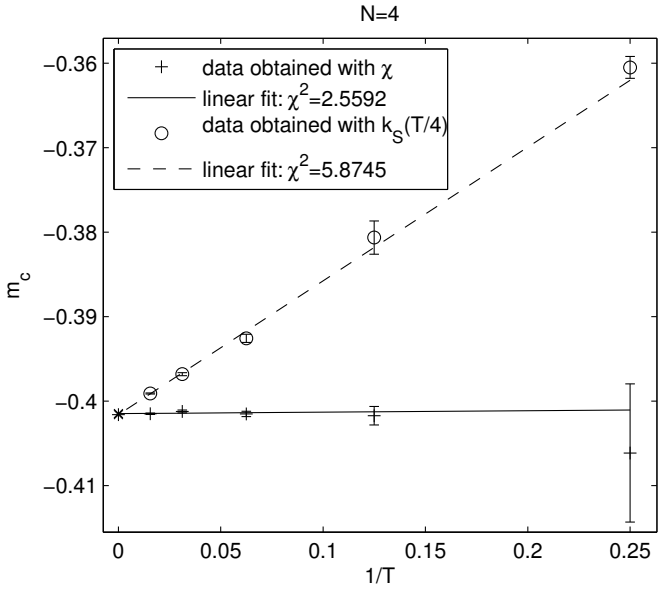


**Figure 5.4:** Critical mass for $T = L = 4, 8, 16, 32, 64$, $N = 4$ and $g^2 = 1/3$. Tuned with $\chi$ and with $k_S(T/4)$. The results of the linear fits are $m_c^{\chi}(T \to \infty) = -0.40149(14)$ and $m_c^{k}(T \to \infty) = -0.40161(11)$.

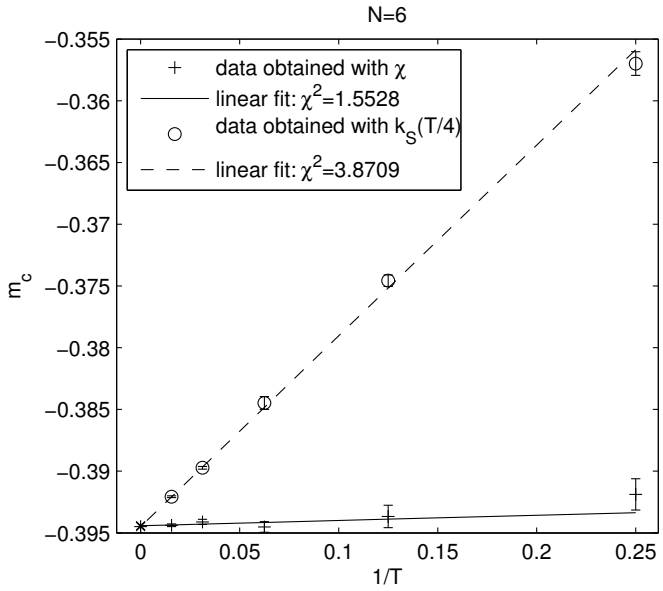


**Figure 5.5:** Critical mass for $T = L = 4, 8, 16, 32, 64$, $N = 6$ and $g^2 = 1/5$. Tuned with $\chi$ and with $k_S(T/4)$. The results of the linear fits are $m_c^{\chi}(T \to \infty) = -0.39442(16)$ and $m_c^{k}(T \to \infty) = -0.394492(86)$.

displayed in figure 5.6. It is close to the leading order perturbation theory prediction [27]

$$\begin{aligned} m_c^{PT} &= -g^2 \cdot K \cdot (N-1) + O(g^4) \\ K &= 0.3849001794598 \ , \end{aligned} \tag{5.9}$$

but it does not agree within the error bounds. For increasing $g^2$ the deviation from the leading order perturbative result also increases. From the lower part of figure 5.6, the corrections can be estimated to be of $O(g^4)$.

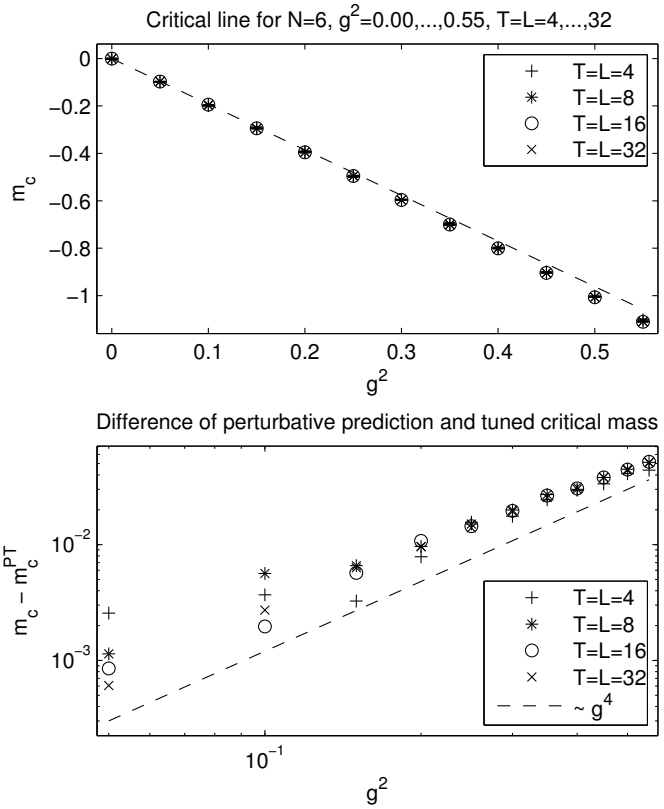


**Figure 5.6:** $N = 6$, $T = L = 8$, $g^2 = 0 \ldots 0.55$: In the upper figure the critical line that was obtained by tuning $\chi(m_c, g^2) = 0$ is displayed for four different lattice sizes. The dashed line is the leading order perturbative result $m_c^{PT}(g^2) \propto g^2 + O(g^4)$. It shows a similar characteristics although it does not agree within the errors. The lower figure shows the discrepancy between the leading order perturbative result and the tuned critical line. The deviations from the leading order perturbative prediction are compatible with $O(g^4)$ (dashed line).

# Chapter 6

# Large N limit

The limit of many flavors $N \to \infty$ is discussed. The derivation follows [7]. The effective potential which determines the leading order saddle point expansion is derived. This potential is seen to undergo a transition from a phase with only one minimum to a phase with two minima as the lattice size exceeds a critical value. For the limit of infinitely many flavors, the critical lattice size can be explicitly calculated while for a finite number of flavors, the critical lattice size is only approximately known. For lattice sizes, and for couplings that are large enough, the transition from one to two minima of the effective potential is also seen in measurements of the monomer density, if the mass is tuned very carefully.

## 6.1 Effective potential

On the lattice, with the Wilson parameter set to $r = 1$, and with the lattice spacing set to $a = 1$, the Gross Neveu partition function reads

$$\begin{aligned} Z &= \int \prod_x \mathrm{d}^{2N}\xi(x) \mathrm{e}^{-\frac{1}{2}\sum_x \xi^T \mathcal{C}(D_W+m)\xi + \frac{g^2}{8}\sum_x (\xi^T\mathcal{C}\xi)^2} \\ D_W &= \tilde{\partial} - \frac{1}{2}\partial_\mu^*\partial_\mu \ . \end{aligned} \tag{6.1}$$

The interaction can be separated with the help of an auxiliary bosonic field. Inserting the constant

$$const. = \int_{-\infty}^{\infty} \prod_x \mathrm{d}\sigma(x) \mathrm{e}^{-\frac{1}{2}\sum_x (\sigma + \frac{g}{2}\xi^T\mathcal{C}\xi)^2} \tag{6.2}$$

into the partition function, and ignoring an irrelevant factor yields

$$Z = \int \prod_x \mathrm{d}\sigma(x) \mathrm{d}^{2N}\xi(x) \mathrm{e}^{-\frac{1}{2}\sum_x \sigma^2 - \frac{1}{2}\xi^T\mathcal{C}[D_W+m+g\sigma]\xi} \ . \tag{6.3}$$

Changing the variables according to

$$g\sigma + m \to \sigma \qquad\qquad g^2 N \to \gamma^2 \ , \tag{6.4}$$

and using the definition of the Pfaffian

$$\mathrm{P}f(A) = \int \mathrm{d}^2\xi \mathrm{e}^{-\frac{1}{2}\xi^T A \xi} \ , \tag{6.5}$$

the partition function can be further rewritten to

$$Z = \int \prod_x \mathrm{d}\sigma(x) \mathrm{e}^{-\frac{N}{2\gamma^2}\sum_x (\sigma - m)^2 + N \log[\mathrm{P}f\{D_W + \sigma\}]} \ . \tag{6.6}$$

For a large number of flavors $N$, the integral in $Z$ is dominated by those $\sigma$ (assumed to be constant) that minimize the effective potential

$$\begin{aligned} V(\sigma) &= \frac{1}{2\gamma^2}(\sigma - m)^2 + V_\xi(\sigma) + O\Big(\frac{1}{N}\Big) \\ V_\xi(\sigma) &= -\log[\mathrm{P}f\{D_W + \sigma\}] = -\frac{1}{2TL}\sum_p \log[\mathring{p}^2 + M_\sigma^2(p)] \ . \end{aligned} \tag{6.7}$$

In the last step the Pfaffian was rewritten by Fourier transformation and the abbreviations (1.23) were used.

In order to examine the characteristics of the potential the derivatives will be needed:

$$\begin{aligned} V(\sigma) &= \frac{(\sigma - m)^2}{2\gamma^2} - \frac{1}{2TL}\sum_p \log[\mathring{p}^2 + M_\sigma^2] \ , \\ V'(\sigma) &= \frac{\sigma - m}{\gamma^2} - \frac{1}{TL}\sum_p \frac{M_\sigma}{\mathring{p}^2 + M_\sigma^2} \ , \\ V''(\sigma) &= \frac{1}{\gamma^2} - \frac{1}{TL}\sum_p \frac{1}{\mathring{p}^2 + M_\sigma^2} + \frac{2}{TL}\sum_p \frac{M_\sigma^2}{(\mathring{p}^2 + M_\sigma^2)^2} \ , \\ V'''(\sigma) &= \frac{6}{TL}\sum_p \frac{M_\sigma}{(\mathring{p}^2 + M_\sigma^2)^2} - \frac{8}{TL}\sum_p \frac{M_\sigma^2}{(\mathring{p}^2 + M_\sigma^2)^3} \ . \end{aligned} \tag{6.8}$$

## 6.2 Symmetry breaking and the triple point renormalization scheme

In the physical range with $\sigma$ close to zero that is considered here [7], the potential can have either one or two minima. There is a point in the parameter space where for fixed lattice size $T$, and for fixed aspect ratio

$$\rho = \frac{L}{T} \tag{6.9}$$

| $T$ | 16 | 32 | 64 | 128 | 256 |
|---|---|---|---|---|---|
| $\gamma^2_{TP1}$ | 3.43394 | 2.49283 | 1.95553 | 1.60858 | 1.36616 |
| $m_{TP1}$ | −1.32174 | −0.95949 | −0.75268 | −0.61914 | −0.52584 |
| $\gamma^2_{TP2}$ | 3.80412 | 2.67826 | 2.06721 | 1.68330 | 1.41966 |
| $m_{TP2}$ | −1.46418 | −1.03086 | −0.79567 | −0.64790 | −0.54643 |
| $\gamma^2_{TP4}$ | 3.82259 | 2.68696 | 2.07233 | 1.68667 | 1.42206 |
| $m_{TP4}$ | −1.47128 | −1.03421 | −0.79764 | −0.64920 | −0.54735 |
| $\gamma^2_{TP8}$ | 3.82262 | 2.68698 | 2.07234 | 1.68668 | 1.42207 |
| $m_{TP8}$ | −1.47130 | −1.03422 | −0.79764 | −0.64920 | −0.54735 |
| $\gamma^2_{TP16}$ | 3.82262 | 2.68698 | 2.07234 | 1.68668 | 1.42207 |
| $m_{TP16}$ | −1.47130 | −1.03422 | −0.79764 | −0.64920 | −0.54735 |

**Table 6.1:** Triple point parameters for $\rho = L/T = 1, 2, 4, 8, 16$. Note that the values for $\rho = 8$ and for $\rho = 16$ do not differ within the accuracy displayed here.

the two minima merge into one. This point will be called triple point (TP) and is characterized by

$$V'(\sigma)|_{TP\rho} = V''(\sigma)|_{TP\rho} = V'''(\sigma)|_{TP\rho} = 0 \ . \tag{6.10}$$

Demanding the triple point to be at $\sigma = 0$ leads to the conditions

$$\begin{aligned} 0 = V'(0) &= \frac{m}{\gamma^2} + V'_\xi(0) \\ 0 = V''(0) &= \frac{1}{\gamma^2} + V''_\xi(0) \end{aligned} \tag{6.11}$$

which can be solved for $\gamma^2$ and $m$ numerically. The parameters which produce a triple point will be denoted with the subscript $TP\rho$ where $\rho$ is the aspect ratio. Some sets of $\gamma^2_{TP\rho}$ and $m_{TP\rho}$ for given $T$ are displayed in table 6.1.

For a fixed $\gamma^2_{TP\rho}$, lattices larger than the lattice size $T$ displayed in table 6.1 have two minima in the effective potential while lattices smaller than $T$ have only one minimum. The lattice size $T$ for which the triple point is found at a certain $\gamma^2_{TP\rho}$ will be called the *critical size* and will be denoted by $T_c$. Figure 6.1 shows the effective potential for $\gamma^2 = \gamma^2_{TP\rho}$ and $m = m_{TP\rho}$ for lattices larger or smaller than the critical lattice size $T_c$. For lattices larger than the critical size, the potential has two minima which are (for $\gamma^2_{TP\rho}$ and for $m_{TP\rho}$) not degenerate. For lattices smaller than the critical size, the potential has one minimum.

To examine whether it is possible to see the effect of symmetry breaking with a finite number of flavors $N$ it is necessary to know how sensitive the occurrence of the two minima is to variations of the parameters $\gamma^2$ and $m$.

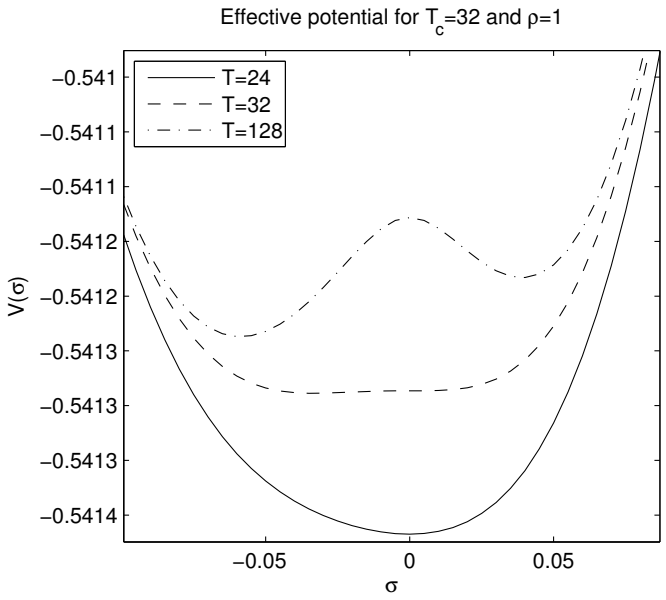


**Figure 6.1:** Effective potential for $T_c = 32$ and $\rho = 1$. The lines show the potential for a lattice size below the critical size ($T = 24$) the critical lattice size ($T = 32$) and a lattice size above the critical size ($T = 128$). For lattices larger than the critical size the potential has two minima which are (for $\gamma^2_{TP\rho}$ and for $m_{TP\rho}$) not degenerate.

The assumption $N \to \infty$ does not necessarily imply that also for finite $N$ the relation

$$\gamma^2 = N \cdot g^2 \tag{6.12}$$

allows for picking a definite $T_c$. Even if (6.12) *approximately* holds, $m$ and $\gamma^2$ will have to be carefully tuned to the critical values which will not exactly coincide with those shown in table 6.1.

Figure 6.2 shows the variation of $m$ or $\gamma^2$ by $\pm 6 \cdot 10^{-3}$ or $\pm 8 \cdot 10^{-3}$ respectively of the critical values. These small variations are large enough to remove one of the minima from the effective potential. Consequently, it can be assumed that only with the mass and/or the coupling tuned with sub-percent accuracy the effect of the two minima can be seen in a measurement at finite $N$.

## 6.3 Measurements

### 6.3.1 Hysteresis

As seen in the previous section, the area in the parameter space where the effective potential has two (almost) degenerate minima is very small. In the

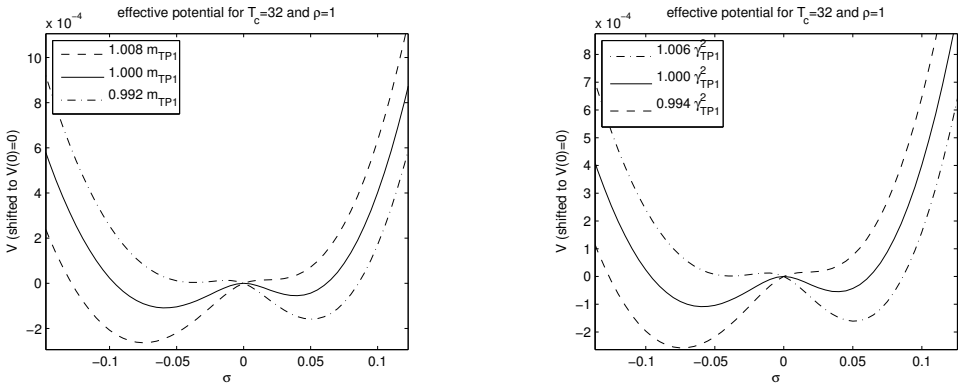


(a) Variation of $m$ by $\pm 8 \cdot 10^{-3} \cdot m_{TP1}$ (b) Variation of $\gamma^2$ by $\pm 6 \cdot 10^{-3} \cdot \gamma^2_{TP1}$

**Figure 6.2:** Effective potential for $T_c = 32$ and $\rho = 1$ at $T = 128$. Variations of $\pm 8 \cdot 10^{-3}$ or $\pm 6 \cdot 10^{-3}$ of the parameters $m$ or $\gamma^2$ already remove one of the minima of the effective potential. It is evident that a careful tuning of $m$ and $\gamma^2$ is necessary to see the effect of symmetry breaking in a Monte Carlo simulation.

following, the coupling constant will be fixed at $g^2 = 0.45$ which for $N = 6$ flavors refers to a critical lattice size between $T = 16$ and $T = 32$ (see table 6.1).

The behavior seen in figure 6.2.a leads to the expectation that (for fixed $\gamma^2$) there is a transition from the situation with one minimum for negative sigma (dashed line) to the situation with one minimum (dash dotted line) if the mass is changed around the critical mass which yields two degenerate minima in the effective potential (solid line). An effect of this transition can be found in the expectation value of the monomer density $K(x)$ measured for a sequence of masses.

When the effective potential has two minima, the loop gas algorithm seems to prevent tunneling between the two minima. As a consequence, there is a critical slowing down close to the critical point, and measurements for a sequence of masses *without thermalization* in between show a hysteresis. Here, this hysteresis will be used to estimate the critical mass. Figure 6.3 shows a part of a sequence of hystereses that has been used to estimate the mass corresponding to the most pronounced double peak in the monomer number.

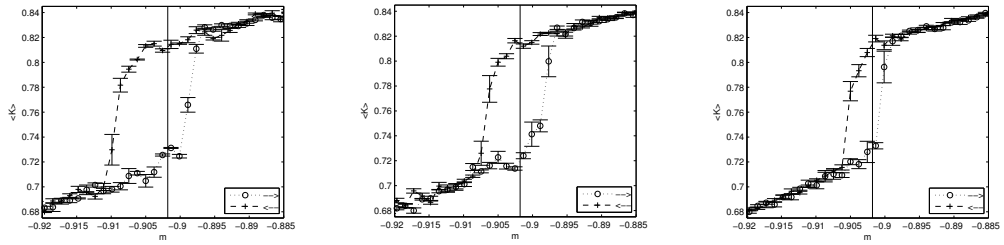


(a) 100 steps per mass (b) 200 steps per mass (c) 400 steps per mass

**Figure 6.3:** Sequence of hystereses for 100, 200 and 400 steps per mass. $T = L = 128$, $N = 6$ and $g^2 = 0.45$. The vertical axis displays the expectation value of the monomer number divided by the number of flavors $N$. The mass shifts are $\delta m = 1.2 \cdot 10^{-}3$. The vertical line represents the mass $m = -0.9018$ that has been found to yield the most pronounced double peak in the monomer number.

### 6.3.2 Two accumulation points of the monomer number

Figure 6.4 shows the monomer number $K$ (normalized to one) for the critical mass. The critical mass has been estimated from a sequence of hystereses as discussed in the previous section. The parameters are $T = L = 128$, $N = 6$, $g^2 = 0.45$, and $m = -0.9018$. They correspond to a critical lattice size $T_c = 16 \ldots 32$ (see table 6.1). There are two accumulation points of the monomer number. One is close to $K = 0.73 \cdot N$ and one is close to $K = 0.8 \cdot N$. The lower part of the figure shows the complete history of the measurement of $K$. Obviously tunneling between the two accumulation points is strongly suppressed. In the whole $1.2 \cdot 10^6$ measurements only about 60 tunneling processes occur. On average, there is one tunneling every $O(10^5)$ Monte Carlo steps. This strong suppression of tunneling indicates slowing down with respect to tunneling (see section 7.2) down above the triple point.

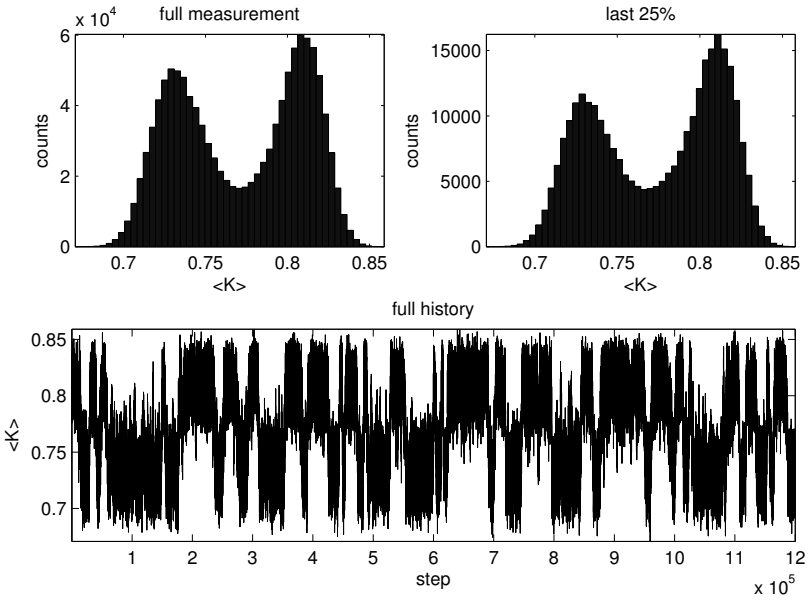


**Figure 6.4:** Monomer number divided by number of flavors $N$ for $T = L = 128$, $N = 6$, $g^2 = 0.45$ (corresponds to $T_c = 16 \ldots 32$), and $m = -0.9018$. The upper part shows the histograms of the monomer density for the full measurement ($1.2 \cdot 10^6$ steps after equally many thermalization steps) and for the last 25% of the measurement. There are two accumulation points for the monomer number. The lower part shows the history of the monomer number for the whole measurement. The system changes from one accumulation point to the other only about 60 times. Tunneling is strongly suppressed and independent measurements can only be expected every $O(10^5)$ steps.

# Chapter 7

# Limitations of the algorithm

Two types of limitations of the algorithm are discussed. First, there are hard constraints which completely forbid simulations for certain areas of the $(m, g^2)$ parameter space. Second, there are limitations which lead to an increase of computer time needed to obtain a certain precision, if the lattice size grows, or if the critical point is approached. These limitations are due to the large condition number of the Dirac operator close to the critical point, and due to the suppression of tunneling processes between the two minima of the effective potential.

## 7.1 Constraints to mass and coupling constant

The range of the coupling constant $g^2$, and of the fermion mass $m$ are constrained by two requirements: the weights $p, q, r$ that eventually govern the bond throwing (see section 2.2.1) have to be non-negative, and the probabilities that are used to pick the auxiliary scalars $\sigma(x)$ also have to be non-negative. Both requirements lead to constraints to the fermion mass, to the coupling constant, or to both the mass and the coupling constant.

### 7.1.1 Constraint stemming from positivity of the bond weights

As $\psi$ replaces $\varphi = 2 + m$ in the effective weight $\rho[k^j; \psi]$ the recursion (2.63) translates to

$$m_K = m_0 + \frac{g^2 K}{2 + m_{K-1}} \ , \qquad m_0 = m \ , \qquad K = 1, \ldots, N-1 \ . \tag{7.1}$$

The assumption that all the "masses" $m_{0,\dots,K-1}$ obey the constraint which ensures positivity of the bond weights

$$-4+\sqrt{8} \leq m_{0,\dots,K-1} \leq \sqrt{8} \tag{7.2}$$

leads to the inequality

$$\frac{1}{\sqrt{8}+2} \leq \frac{1}{2+m_{K-1}} \leq \frac{1}{\sqrt{8}-2} \ . \tag{7.3}$$

As also $m_K$ is required to obey (7.1), the upper and the lower bound of $m$ for a given $g^2$ follow:

$$\begin{aligned} m = m_0 &\leq \sqrt{8} - \frac{g^2 n}{\sqrt{8}-2} \leq \sqrt{8} - \frac{g^2(N-1)}{\sqrt{8}-2} \\ m = m_0 &\geq -4+\sqrt{8} - \frac{g^2 n}{\sqrt{8}+2} \geq -4+\sqrt{8} - \frac{g^2(N-1)}{\sqrt{8}+2} \end{aligned} \tag{7.4}$$

The lower bound is weaker than (7.2), which is why the bounds

$$-4+\sqrt{8} \leq m = m_0 \leq \sqrt{8} - \frac{g^2(N-1)}{\sqrt{8}-2} \tag{7.5}$$

make sure that all weights are positive.

### 7.1.2 Constraint stemming from the solver

The requirement that the weights (3.6) are non-negative yields the constraint

$$\begin{aligned} m = m_0 &\geq -g\sigma_i - 2 \\ m = m_0 &\geq -g \min_i \sigma_i - 2 \ . \end{aligned} \tag{7.6}$$

The minimal $\sigma_i$ depend on the number of flavors $N$. This constraint will be the first to interfere with the critical line when the coupling $g^2$ is increased.

### 7.1.3 Visualization of the constraints

In figure 7.1, the $m$-$g^2$-plane is displayed for $N = 6$ and for $N = 8$ flavors. The gray areas are forbidden by the constraints stemming from the bond weights and from the solver. Furthermore, the leading order prediction for the critical line $m_c(g^2)$ (see section 5.4), and the coupling constants which approximate the triple point (see section 6.2) above which there are two minima in the effective potential is displayed for different lattice sizes.

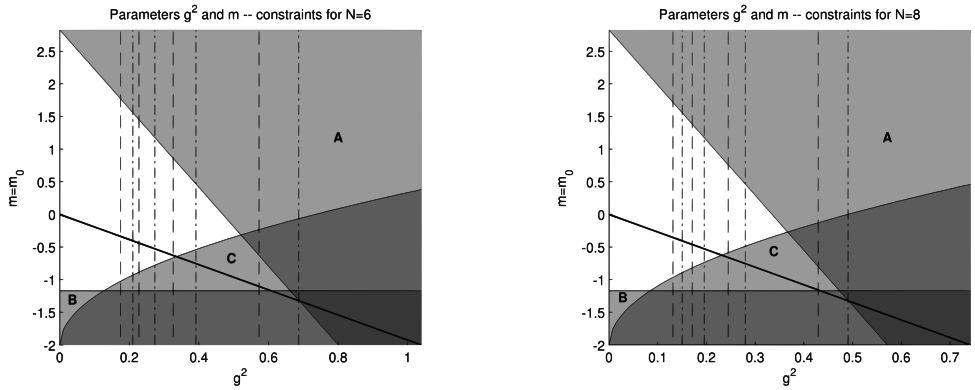


(a) 6 flavors (b) 8 flavors

**Figure 7.1:** Visualization of constraints to pairs $(m, g^2)$ for $N = 6$ and for $N = 8$ flavors. The gray areas are forbidden. Constraint **A** stems from positivity of the weights $p, q, r$ for positive (effective) masses obtained from the recursion (7.1). Constraint **B** stems from the same requirement for negative masses obtained from the recursion. Constraint **C** stems from positivity of the effective weights from the Hermite integration. The solid line represents the leading order perturbative prediction for $m(g^2)$. The vertical lines are the triple point couplings $g^2_{TP}(T_c)$ estimated with $\gamma^2_{TP} = N\, g^2_{TP}$ (dashed line) and with $\gamma^2_{TP} = (N-1)\, g^2_{TP}$ (dash-dotted line). Starting from the left, the triple point couplings for $T_c = 1024, 256, 64, \ldots$ are displayed.

From the visualization of the constraints it is evident that the constraint stemming from the solver interferes with the critical line before the others do. And, for increasing $N$, the area of $(m, g^2)$ covered by the algorithm gets smaller. However, the triple point is reachable for smaller and smaller lattices, as $N$ increases.

## 7.2 Critical slowing down beyond the triple point

Above the triple point (e.g. in the region of the parameter space where there can be two minima in the effective potential), the loop gas algorithm becomes inefficient with regard to tunneling between the two minima of the effective potential (see figure 6.4). However, there may be quantities which are not sensitive to this tunneling process, and which then will not suffer from critical slowing down[1].

[1]Think of the Ising model without external magnetic field far in the ordered phase: The Metropolis algorithm is very inefficient in flipping the whole system, and hence will suffer from large autocorrelation times for the magnetization (no modulus!). On the other

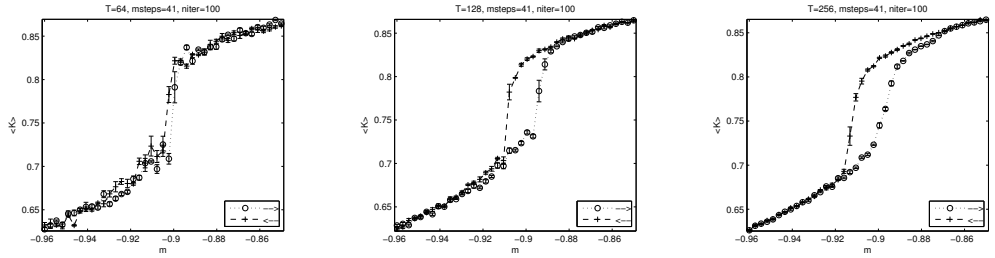


(a) $T = L = 64$ (b) $T = L = 128$ (c) $T = L = 256$

**Figure 7.2:** Monomer number for $T = L = 65, 128, 256$, $N = 6$ and $g^2 = 0.45$. The data points were obtained from 100 measurements per mass. The mass shifts are $2.7 \cdot 10^3$. With increasing lattice size the area of the hysteresis becomes larger.

As seen in section 6.3, the monomer number measured for a sequence of masses around the critical mass without thermalization in between follows a hysteresis. Figure 7.2 displays the hysteresis of the monomer number for different lattice sizes. The area of the hysteresis increases with increasing lattice size. The area of the hysteresis is a measure for the ability of the algorithm to produce configurations that correspond to one accumulation point from configurations that correspond to the other accumulation point: The larger the hysteresis, the "slower" the tunneling between the two accumulation point, and the larger the autocorrelation between subsequent measurements. This fact was also illustrated in the lower part of figure 6.4, where over a history of $1.2 \cdot 10^6$ measurements only about 60 tunneling processes between the two accumulation points occurred.

## 7.3 Convergence of the solver

As discussed in section 3.2, the Green's function is measured by iterative inversion of the Dirac operator using the conjugate gradient method. Unfortunately, the convergence of the solver was very poor: The number of iterations needed to obtain the desired precision increases linearly with the size of the lattice $T$. Figure 7.3(a) displays the number of iterations that are necessary to obtain a (rather moderate) precision of $10^{-5}$ (norm of residue vector). It reveals that the number of iterations are proportional to the lattice size. The mass influences the convergence in such a way that, the closer the system is to the critical point, the more iterations are needed. Figure 7.3(b)

hand, the energy does not depend on the overall sign of the spins, and the Metropolis algorithm will still yield small autocorrelation times for the energy.

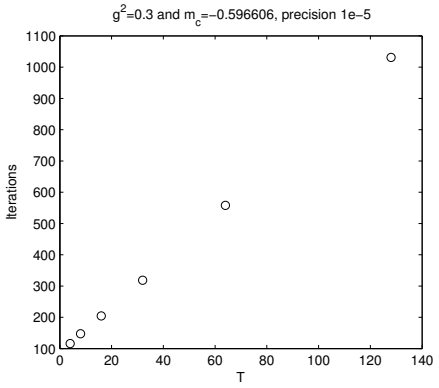


(a) Precision $10^{-5}$, $T = L = 4 \ldots 128$, $m = -0.596606 \approx m_c$. The number of iterations rises linearly with the lattice size $T$.

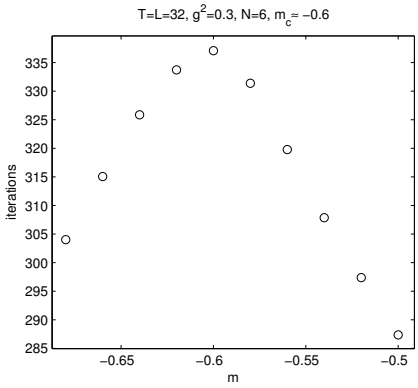


(b) Precision $10^{-11}$, $T = L = 32$, $m = -0.68 \ldots -0.5$. The number of iterations rises, as the system approaches the critical point.

**Figure 7.3:** Number of iterations which are necessary to obtain the desired precision (norm of the residue vector). $N = 6$, $g^2 = 0.3$, $m_c = -0.596606$.

shows that, the number of iterations is maximal at the critical point. Furthermore, it has been found that the number of flavors $N$ does not influence the convergence, and the number of iterations.

As the size of the matrix that is inverted rises with $T^2$, it can be assumed that the computation time per iteration also rises proportional to $T^2$. Altogether, an increase in computation time proportional to $T^3$ is assumed, and time measurements confirm this assumption. Time measurements on one core of an Intel Quad CPU running at $2.66GHz$ showed that one solve with precision $10^{-5}$ needs about 110 seconds. Doubling the desired precision to $10^{-10}$ increases the computation time to 150 seconds. Within a month, less than 20 000 inversions could be accumulated, rendering precision measurements on lattices larger than $T = 256$ (which are necessary to simulate far in the broken phase, see figure 7.1) tedious.

# Conclusions

In the first chapter of this thesis, the Gross Neveu model was introduced. The model was discretized in terms of Wilson fermions, and the fact that this discretization breaks the chiral symmetry of the model was discussed briefly.

The second chapter described the reformulation of the fermion partition function in terms of dimer variables, which live on the links. The loop gas algorithm was derived first for free and then for interacting fermions. Then, a chapter on observables followed. The measurement of Green's functions was discussed, and the scalar correlation, which later provided a definition of the critical mass was derived.

In chapter four, the algorithm was tested against exactly known results for the free fermion propagator. A brief test of the algorithm's sensitivity to the choice of random numbers followed.

Chapter five examined the critical mass of the model. Two different definitions of the critical mass were compared and were found to be compatible in the infinite volume limit. Then, the computationally more favorable definition of the critical point was used to measure the critical line. A comparison to the leading order perturbative prediction revealed qualitative agreement up to corrections which are consistent with the next order.

In chapter six, a brief compilation of a large $N$ calculation was presented. The prediction of two degenerate minima of the effective potential could be observed for finite $N$. The algorithm was found to have large autocorrelation times with regard to tunneling between the two minima of the potential.

The last chapter contained an overview of the limitations of the algorithm. A set of hard constraints to the parameters (mass and coupling) which can be handled by the algorithm were discussed, and the computational necessary effort to measure correlation functions at growing lattice size was estimated.

During the last months of this work, a new approach to the dimer formulation of fermions was developed by Ulli Wolff. For free Wilson fermions, an algorithm based on the worm algorithm [28, 29] was presented [30]. This new approach samples two point functions in a very natural way, and, as

no inversion of the Dirac operator is needed, there is hope that correlation functions can be measured with much less computational effort.

# Appendix A

# Ensembles and expectation values

## A.1 Ensembles

- Free Majorana Wilson fermions with boundary conditions $\epsilon$

$$Z_\xi^\epsilon[\varphi] = \int \mathrm{D}\xi \, \mathrm{e}^{-\frac{1}{2}\sum_x \varphi(x)\xi^T(x)\mathcal{C}\xi(x) + \sum_{x,\mu} \xi^T(x)\mathcal{C}P(\hat{\mu})\xi(x+\hat{\mu})} \tag{A.1}$$

- Free single flavor ($N = 1$) positive weight loop ensemble
  - All topologies

$$Z_k[\varphi] = \sum_{\{k\}} \rho[k;\varphi] \tag{A.2}$$

  - Projected to topology $e'$

$$Z_k^{e'}[\varphi] = \sum_{\{k\}} \rho[k;\varphi]\delta_{e[k],e'} \tag{A.3}$$

- $N$ flavor Majorana Wilson fermions with Gross Neveu interaction and boundary conditions distributed according to $z^i(\epsilon)$ for flavor $i$
  - Definition (Gaussian measure $\mathrm{d}\mu(\sigma)$)

$$Z_{GN}^{\{z^i\}} = \int \prod_x \mathrm{d}\mu(\sigma(x)) \prod_{i=1}^N Z_\xi^{z^i}[\varphi + g\sigma] \quad Z_\xi^z = \sum_\epsilon z(\epsilon) Z_\xi^\epsilon \tag{A.4}$$

  - Loop representation

$$Z_{GN}^{\{z^i\}} = \sum_{\{k^1\},\{k^2\},\ldots} \left[\prod_{i=1}^N \rho[k^i;\varphi]\Phi[e^i;z^i]\right] \prod_x c(K(x),\varphi,g) \tag{A.5}$$

– Mixed form

$$Z^{\{z^i\}}_{GN,\sigma} = \int \prod_x \mathrm{d}\mu(\sigma(x)) \sum_{\{k^1\},\{k^2\},\ldots} \left[\prod_{i=1}^{N} \rho[k^i;\varphi]\Phi[e^i;z^i]\right] \times \\ \times \prod_x \frac{\varphi(x)+g\sigma(x)}{c(K(x),\varphi,g)} c(K(x),\varphi,g) \quad \text{(A.6)}$$

- $N$ flavor Majorana Wilson fermions with Gross Neveu interaction and positive weights

  – Loop representation

$$Z_\rho = \sum_{\{k^1\},\{k^2\},\ldots} \left[\prod_{i=1}^{N} \rho[k^i;\varphi]\right] \prod_x c(K(x),\varphi,g) \quad \text{(A.7)}$$

  – Mixed form

$$Z_{\rho,\sigma} = \int \prod_x \mathrm{d}\mu(\sigma(x)) \sum_{\{k^1\},\{k^2\},\ldots} \left[\prod_{i=1}^{N} \rho[k^i;\varphi]\right] \times \\ \times \prod_x \frac{\varphi(x)+g\sigma(x)}{c(K(x),\varphi,g)} c(K(x),\varphi,g) \quad \text{(A.8)}$$

## A.2 Expectation values

The corresponding expectation values carry the same sub- and superscripts. For example, $\langle \ldots \rangle_k$ corresponds to the free loop ensemble with positive weights $Z_k[\varphi]$.

## A.3 Reweighting between the ensembles

- $Z_k$ vs. $Z^e_k$

$$Z_k[\varphi] = \sum_e Z^e_k[\varphi] \quad \text{(A.9)}$$

- $Z^\epsilon_\xi$ vs. $Z_k$ and $Z^e_k$

$$\begin{aligned} Z^\epsilon_\xi[\varphi] &= \sum_e Z^e_k[\varphi]\Phi[e;\epsilon] \\ Z_k[\varphi] &= \frac{1}{4}\sum_{e,\epsilon} Z^\epsilon_\xi[\varphi]\Phi[e;\epsilon] \\ \langle A\rangle^\epsilon_\xi &= \frac{\langle A\Phi[e,\epsilon]\rangle_k}{\langle \Phi[e,\epsilon]\rangle_k} \end{aligned} \quad \text{(A.10)}$$

- $Z^{\{z^i\}}_{GN,(\sigma)}$ vs. $Z_{\rho,(\sigma)}$

$$
\begin{aligned}
Z^{\{z^i\}}_{GN,(\sigma)}[\varphi] &= Z_{\rho,(\sigma)} \left\langle \prod_{i=1}^{N} \Phi[e^i; z^i] \right\rangle_{\rho} \\
\langle A \rangle^{\{z^i\}}_{GN,(\sigma)} &= \frac{\left\langle A \prod_{i=1}^{N} \Phi[e^i; z^i] \right\rangle_{\rho,(\sigma)}}{\left\langle \prod_{i=1}^{N} \Phi[e^i; z^i] \right\rangle_{\rho}}
\end{aligned}
\tag{A.11}
$$

# Appendix B

# Data: Tuning with $\chi$ for $N = 6$

**Table B.1:** $N = 6$, $T = L = 4$, $10^6$ steps per $m$. Errors are ($statistic + systematic$).

| $g^2$ | $m$ | $\chi$ |
|---|---|---|
| 0.00000 | $-0.011562500000000$ | $-0.00619(52)$ |
| 0.00000 | $-0.007021564124434$ | $-0.00381(52)$ |
| 0.00000 | $-0.002480628248868$ | $-0.00133(53)$ |
| 0.00000 | $+0.006142498375566$ | $+0.00335(55)$ |
| 0.00000 | $+0.014765625000000$ | $+0.00884(57)$ |
| | $m_c = -0.00033(42 + 44)$ | |
| 0.05000 | $-0.103710937500000$ | $-0.00418(53)$ |
| 0.05000 | $-0.099679899954604$ | $-0.00027(54)$ |
| 0.05000 | $-0.095648862409209$ | $+0.00080(54)$ |
| 0.05000 | $-0.093097868704604$ | $+0.00243(55)$ |
| 0.05000 | $-0.090546875000000$ | $+0.00361(55)$ |
| | $m_c = -0.09738(44 + 77)$ | |
| 0.10000 | $-0.198729511920155$ | $-0.00216(54)$ |
| 0.10000 | $-0.196660494160586$ | $-0.00171(54)$ |
| 0.10000 | $-0.194591476401017$ | $-0.00018(55)$ |
| 0.10000 | $-0.189360928680547$ | $+0.00169(55)$ |
| 0.10000 | $-0.184130380960077$ | $+0.00547(57)$ |
| | $m_c = -0.19389(48 + 75)$ | |
| 0.15000 | $-0.301171875000000$ | $-0.00508(53)$ |
| 0.15000 | $-0.296580448951791$ | $-0.00229(54)$ |
| 0.15000 | $-0.291989022903583$ | $+0.00102(56)$ |
| 0.15000 | $-0.289998417701791$ | $+0.00112(56)$ |
| 0.15000 | $-0.288007812500000$ | $+0.00259(56)$ |
| | $m_c = -0.29264(43 + 35)$ | |

**Table B.1:** Continued.

| $g^2$ | $m$ | $\chi$ |
|---|---|---|
| 0.20000 | −0.406484375000000 | −0.00679(53) |
| 0.20000 | −0.399452893849132 | −0.00423(54) |
| 0.20000 | −0.392421412698265 | +0.00054(56) |
| 0.20000 | −0.386288831349132 | +0.00213(56) |
| 0.20000 | −0.380156250000000 | +0.00607(58) |
| | $m_c = -0.39201(51 + 27)$ | |
| 0.25000 | −0.498632812500000 | −0.00374(55) |
| 0.25000 | −0.495305344977384 | −0.00193(56) |
| 0.25000 | −0.491977877454767 | +0.00031(56) |
| 0.25000 | −0.488723313727384 | +0.00158(56) |
| 0.25000 | −0.485468750000000 | +0.00356(58) |
| | $m_c = -0.49194(46 + 13)$ | |
| 0.30000 | −0.643437500000000 | −0.02291(47) |
| 0.30000 | −0.619965071097883 | −0.01229(52) |
| 0.30000 | −0.596492642195767 | −0.00172(56) |
| 0.30000 | −0.567308821097883 | +0.01395(62) |
| 0.30000 | −0.538125000000000 | +0.03235(68) |
| | $m_c = -0.5967(05 + 32)$ | |
| 0.35000 | −0.702886149390243 | −0.00385(56) |
| 0.35000 | −0.698411323846765 | −0.00294(56) |
| 0.35000 | −0.693936498303286 | −0.00108(57) |
| 0.35000 | −0.690980242672984 | +0.00196(58) |
| 0.35000 | −0.688023987042683 | +0.00254(58) |
| | $m_c = -0.69339(57 + 73)$ | |
| 0.40000 | −0.801406250000000 | −0.00355(57) |
| 0.40000 | −0.798303865799623 | −0.00161(58) |
| 0.40000 | −0.795201481599246 | +0.00047(58) |
| 0.40000 | −0.791721834549623 | +0.00217(59) |
| 0.40000 | −0.788242187500000 | +0.00386(59) |
| | $m_c = -0.79545(46 + 37)$ | |
| 0.45000 | −0.906718750000000 | −0.00479(56) |
| 0.45000 | −0.901255443752836 | −0.00149(58) |
| 0.45000 | −0.895792137505672 | +0.00065(58) |
| 0.45000 | −0.888091381252836 | +0.00469(61) |
| 0.45000 | −0.880390625000000 | +0.00838(62) |
| | $m_c = -0.89746(55 + 14)$ | |
| 0.50000 | −1.012031250000000 | −0.00620(56) |
| 0.50000 | −1.006820024846538 | −0.00380(57) |

**Table B.1:** Continued.

| $g^2$ | $m$ | $\chi$ |
|---|---|---|
| 0.50000 | −1.001608799693077 | −0.00051(59) |
| 0.50000 | −0.993655962346538 | +0.00196(60) |
| 0.50000 | −0.985703125000000 | +0.00729(62) |
| | $m_c = -0.99945(53 + 38)$ | |
| 0.55000 | −1.117343750000000 | −0.00691(57) |
| 0.55000 | −1.109525564799585 | −0.00456(58) |
| 0.55000 | −1.101707379599169 | +0.00081(61) |
| 0.55000 | −1.096361502299585 | +0.00384(62) |
| 0.55000 | −1.091015625000000 | +0.00560(63) |
| | $m_c = -1.10270(53 + 34)$ | |

**Table B.2:** $N = 6$, $T = L = 8$, $10^6$ steps per $m$. Errors are (*statistic* + *systematic*).

| $g^2$ | $m$ | $\chi$ |
|---|---|---|
| 0.00000 | −0.002882776976142 | −0.00401(55) |
| 0.00000 | −0.001515833033960 | −0.00176(56) |
| 0.00000 | −0.000148889091778 | −0.00001(56) |
| 0.00000 | +0.000690217213058 | +0.00111(57) |
| 0.00000 | +0.001529323517894 | +0.00246(57) |
| | $m_c = -0.00016(18 + 03)$ | |
| 0.05000 | −0.103710937500000 | −0.00695(55) |
| 0.05000 | −0.101008595749578 | −0.00519(55) |
| 0.05000 | −0.098306253999156 | −0.00132(57) |
| 0.05000 | −0.094426564499578 | +0.00266(58) |
| 0.05000 | −0.090546875000000 | +0.00840(61) |
| | $m_c = -0.09718(22 + 48)$ | |
| 0.10000 | −0.196704002274662 | −0.00245(58) |
| 0.10000 | −0.195882820495547 | −0.00078(58) |
| 0.10000 | −0.195061638716432 | −0.00076(58) |
| 0.10000 | −0.193941909618785 | +0.00103(59) |
| 0.10000 | −0.192822180521139 | +0.00333(60) |
| | $m_c = -0.19494(19 + 21)$ | |
| 0.15000 | −0.301171875000000 | −0.00812(57) |
| 0.15000 | −0.297551832555208 | −0.00549(58) |
| 0.15000 | −0.293931790110415 | −0.00097(60) |
| 0.15000 | −0.290969801305208 | +0.00509(62) |
| 0.15000 | −0.288007812500000 | +0.00777(63) |
| | $m_c = -0.29405(21 + 52)$ | |

**Table B.2:** Continued.

| $g^2$ | $m$ | $\chi$ |
|---|---|---|
| 0.20000 | −0.406484375000000 | −0.01595(54) |
| 0.20000 | −0.400947721975850 | −0.00837(58) |
| 0.20000 | −0.395411068951701 | −0.00106(61) |
| 0.20000 | −0.387783659475850 | +0.00822(65) |
| 0.20000 | −0.380156250000000 | +0.01979(70) |
| | $m_c = -0.39455(21 + 16)$ | |
| 0.25000 | −0.498632812500000 | −0.00379(62) |
| 0.25000 | −0.497183198310599 | −0.00303(62) |
| 0.25000 | −0.495733584121197 | −0.00197(63) |
| 0.25000 | −0.493892182685599 | +0.00207(65) |
| 0.25000 | −0.492050781250000 | +0.00444(65) |
| | $m_c = -0.49515(22 + 46)$ | |
| 0.30000 | −0.603945312500000 | −0.01039(61) |
| 0.30000 | −0.600771020338446 | −0.00484(63) |
| 0.30000 | −0.597596728176891 | −0.00112(65) |
| 0.30000 | −0.594188989088446 | +0.00228(67) |
| 0.30000 | −0.590781250000000 | +0.00838(69) |
| | $m_c = -0.59662(22 + 04)$ | |
| 0.35000 | −0.702675781250000 | −0.00730(64) |
| 0.35000 | −0.700466088793047 | −0.00206(67) |
| 0.35000 | −0.698256396336094 | +0.00050(68) |
| 0.35000 | −0.697175073168047 | +0.00182(69) |
| 0.35000 | −0.696093750000000 | +0.00352(70) |
| | $m_c = -0.69849(20 + 39)$ | |
| 0.40000 | −0.803275454074087 | −0.00452(68) |
| 0.40000 | −0.801923034565703 | −0.00216(69) |
| 0.40000 | −0.800570615057320 | −0.00106(69) |
| 0.40000 | −0.799451493431443 | +0.00134(71) |
| 0.40000 | −0.798332371805565 | +0.00374(72) |
| | $m_c = -0.80038(20 + 18)$ | |
| 0.45000 | −0.906718750000000 | −0.00528(70) |
| 0.45000 | −0.904972074484304 | −0.00250(71) |
| 0.45000 | −0.903225398968607 | −0.00032(73) |
| 0.45000 | −0.901681058859304 | +0.00260(74) |
| 0.45000 | −0.900136718750000 | +0.00384(75) |
| | $m_c = -0.90311(23 + 14)$ | |
| 0.50000 | −1.012031250000000 | −0.00917(70) |
| 0.50000 | −1.008530864460850 | −0.00430(73) |

**Table B.2:** Continued.

| $g^2$ | $m$ | $\chi$ |
|---|---|---|
| 0.50000 | $-1.005030478921700$ | $+0.00075(75)$ |
| 0.50000 | $-1.001948833210850$ | $+0.00769(81)$ |
| 0.50000 | $-0.998867187500000$ | $+0.01060(82)$ |
| | $m_c = -1.00598(22 + 06)$ | |
| 0.55000 | $-1.117343750000000$ | $-0.01370(69)$ |
| 0.55000 | $-1.114012715602906$ | $-0.00880(74)$ |
| 0.55000 | $-1.110681681205813$ | $-0.00251(78)$ |
| 0.55000 | $-1.107430684352907$ | $+0.00226(80)$ |
| 0.55000 | $-1.104179687500000$ | $+0.00881(85)$ |
| | $m_c = -1.10909(23 + 15)$ | |

**Table B.3:** $N = 6$, $T = L = 16$, $10^6$ steps per $m$. Errors are $(statistic + systematic)$.

| $g^2$ | $m$ | $\chi$ |
|---|---|---|
| 0.00000 | $-0.001689453125000$ | $-0.00482(56)$ |
| 0.00000 | $-0.000650821910171$ | $-0.00138(58)$ |
| 0.00000 | $+0.000387809304658$ | $+0.00112(59)$ |
| 0.00000 | $+0.000994685902329$ | $+0.00176(59)$ |
| 0.00000 | $+0.001601562500000$ | $+0.00276(59)$ |
| | $m_c = +0.00018(11 + 27)$ | |
| 0.05000 | $-0.103710937500000$ | $-0.01665(53)$ |
| 0.05000 | $-0.100560211049301$ | $-0.00884(56)$ |
| 0.05000 | $-0.097409484598601$ | $-0.00111(60)$ |
| 0.05000 | $-0.093978179799301$ | $+0.00817(63)$ |
| 0.05000 | $-0.090546875000000$ | $+0.01750(67)$ |
| | $m_c = -0.09717(10 + 13)$ | |
| 0.10000 | $-0.195859375000000$ | $-0.00317(61)$ |
| 0.10000 | $-0.195460908537190$ | $-0.00134(62)$ |
| 0.10000 | $-0.195062442074380$ | $-0.00023(63)$ |
| 0.10000 | $-0.194638154630940$ | $+0.00106(63)$ |
| 0.10000 | $-0.194213867187500$ | $+0.00338(64)$ |
| | $m_c = -0.195031(74 + 32)$ | |
| 0.15000 | $-0.296721492698603$ | $-0.00594(63)$ |
| 0.15000 | $-0.295683698329117$ | $-0.00402(64)$ |
| 0.15000 | $-0.294645903959630$ | $-0.00096(65)$ |
| 0.15000 | $-0.293458507178418$ | $+0.00161(66)$ |
| 0.15000 | $-0.292271110397206$ | $+0.00679(69)$ |
| | $m_c = -0.29437(11 + 23)$ | |

**Table B.3:** Continued.

| $g^2$ | $m$ | $\chi$ |
|---|---|---|
| 0.20000 | −0.396360653276787 | −0.00683(65) |
| 0.20000 | −0.395304805758298 | −0.00275(67) |
| 0.20000 | −0.394248958239810 | +0.00120(70) |
| 0.20000 | −0.393279255348700 | +0.00348(70) |
| 0.20000 | −0.392309552457590 | +0.00627(72) |
| | $m_c = -0.39438(10 + 15)$ | |
| 0.25000 | −0.498632812500000 | −0.01123(67) |
| 0.25000 | −0.496957164243467 | −0.00433(71) |
| 0.25000 | −0.495281515986934 | −0.00045(73) |
| 0.25000 | −0.493666148618467 | +0.00560(76) |
| 0.25000 | −0.492050781250000 | +0.01088(80) |
| | $m_c = -0.495344(100 + 31)$ | |
| 0.30000 | −0.603945312500000 | −0.02258(63) |
| 0.30000 | −0.600849344084211 | −0.01299(70) |
| 0.30000 | −0.597753375668421 | −0.00252(78) |
| 0.30000 | −0.594267312834211 | +0.00813(84) |
| 0.30000 | −0.590781250000000 | +0.02342(92) |
| | $m_c = -0.59713(11 + 28)$ | |
| 0.35000 | −0.702675781250000 | −0.01382(75) |
| 0.35000 | −0.700745388150496 | −0.00740(79) |
| 0.35000 | −0.698814995050993 | −0.00164(84) |
| 0.35000 | −0.697454372525496 | +0.00450(89) |
| 0.35000 | −0.696093750000000 | +0.00993(91) |
| | $m_c = -0.69868(11 + 15)$ | |
| 0.40000 | −0.802495523769903 | −0.00585(90) |
| 0.40000 | −0.801653135052776 | −0.00258(91) |
| 0.40000 | −0.800810746335648 | −0.00065(92) |
| 0.40000 | −0.800160203836945 | +0.00283(95) |
| 0.40000 | −0.799509661338242 | +0.00452(98) |
| | $m_c = -0.80083(12 + 02)$ | |
| 0.45000 | −0.906718750000000 | −0.01194(91) |
| 0.45000 | −0.905098170148302 | −0.00664(97) |
| 0.45000 | −0.903477590296604 | +0.00064(103) |
| 0.45000 | −0.901807154523302 | +0.00419(105) |
| 0.45000 | −0.900136718750000 | +0.01455(114) |
| | $m_c = -0.90348(12 + 20)$ | |
| 0.50000 | −1.012031250000000 | −0.02212(89) |
| 0.50000 | −1.009454037675739 | −0.01399(96) |

**Table B.3:** Continued.

| $g^2$ | $m$ | $\chi$ |
|---|---|---|
| 0.50000 | $-1.006876825351478$ | $-0.00328(111)$ |
| 0.50000 | $-1.002872006425739$ | $+0.01500(128)$ |
| 0.50000 | $-0.998867187500000$ | $+0.04005(149)$ |
| | $m_c = -1.00668(11 + 67)$ | |
| 0.55000 | $-1.110761718750000$ | $-0.0074(12)$ |
| 0.55000 | $-1.109827821294731$ | $-0.0043(12)$ |
| 0.55000 | $-1.108893923839463$ | $-0.0001(13)$ |
| 0.55000 | $-1.108182313482232$ | $+0.0038(13)$ |
| 0.55000 | $-1.107470703125000$ | $+0.0057(13)$ |
| | $m_c = -1.10892(14 + 03)$ | |

**Table B.4:** $N = 6$, $T = L = 32$, $10^6$ steps per $m$. Errors are ($statistic + systematic$).

| $g^2$ | $m$ | $\chi$ |
|---|---|---|
| 0.00000 | $-0.001689453125000$ | $-0.00875(56)$ |
| 0.00000 | $-0.001038933812429$ | $-0.00582(57)$ |
| 0.00000 | $-0.000388414499857$ | $-0.00223(59)$ |
| 0.00000 | $+0.000606574000071$ | $+0.00269(61)$ |
| 0.00000 | $+0.001601562500000$ | $+0.00893(63)$ |
| | $m_c = +0.000013(51 + 68)$ | |
| 0.05000 | $-0.098550227673170$ | $-0.00912(59)$ |
| 0.05000 | $-0.097730797213137$ | $-0.00363(61)$ |
| 0.05000 | $-0.096911366753104$ | $+0.00051(63)$ |
| 0.05000 | $-0.095729959044845$ | $+0.00653(66)$ |
| 0.05000 | $-0.094548551336585$ | $+0.01316(68)$ |
| | $m_c = -0.096966(52 + 42)$ | |
| 0.10000 | $-0.195859375000000$ | $-0.00460(65)$ |
| 0.10000 | $-0.195423585288517$ | $-0.00374(66)$ |
| 0.10000 | $-0.194987795577033$ | $-0.00094(66)$ |
| 0.10000 | $-0.194600831382267$ | $+0.00112(68)$ |
| 0.10000 | $-0.194213867187500$ | $+0.00538(70)$ |
| | $m_c = -0.19492(05 + 13)$ | |
| 0.15000 | $-0.294589843750000$ | $-0.00318(70)$ |
| 0.15000 | $-0.294389013559338$ | $-0.00164(71)$ |
| 0.15000 | $-0.294188183368677$ | $-0.00015(72)$ |
| 0.15000 | $-0.293977636606213$ | $+0.00169(74)$ |
| 0.15000 | $-0.293767089843750$ | $+0.00334(74)$ |
| | $m_c = -0.294184(40 + 06)$ | |

**Table B.4:** Continued.

| $g^2$ | $m$ | $\chi$ |
|---|---|---|
| 0.20000 | $-0.394965820312500$ | $-0.00509(75)$ |
| 0.20000 | $-0.394584443560956$ | $-0.00448(76)$ |
| 0.20000 | $-0.394203066809412$ | $-0.00016(79)$ |
| 0.20000 | $-0.393761689654706$ | $+0.00400(82)$ |
| 0.20000 | $-0.393320312500000$ | $+0.00822(84)$ |
| | $m_c = -0.394225(42 + 94)$ | |
| 0.25000 | $-0.496120338069886$ | $-0.00791(83)$ |
| 0.25000 | $-0.495619574960869$ | $-0.00603(84)$ |
| 0.25000 | $-0.495118811851851$ | $+0.00082(89)$ |
| 0.25000 | $-0.494602185755897$ | $+0.00427(93)$ |
| 0.25000 | $-0.494085559659943$ | $+0.00816(96)$ |
| | $m_c = -0.495091(48 + 11)$ | |
| 0.30000 | $-0.597363281250000$ | $-0.00580(95)$ |
| 0.30000 | $-0.597034335060892$ | $-0.00332(100)$ |
| 0.30000 | $-0.596705388871785$ | $-0.00198(100)$ |
| 0.30000 | $-0.596211581154642$ | $+0.00410(106)$ |
| 0.30000 | $-0.595717773437500$ | $+0.00701(108)$ |
| | $m_c = -0.596606(57 + 26)$ | |
| 0.35000 | $-0.699384765625000$ | $-0.0063(11)$ |
| 0.35000 | $-0.698900235520697$ | $-0.0032(12)$ |
| 0.35000 | $-0.698415705416395$ | $+0.0011(12)$ |
| 0.35000 | $-0.698077481614447$ | $+0.0045(12)$ |
| 0.35000 | $-0.697739257812500$ | $+0.0059(13)$ |
| | $m_c = -0.698556(69 + 02)$ | |
| 0.40000 | $-0.801622862944874$ | $-0.0075(13)$ |
| 0.40000 | $-0.801294767056780$ | $-0.0074(13)$ |
| 0.40000 | $-0.800966671168687$ | $-0.0008(14)$ |
| 0.40000 | $-0.800493663072767$ | $+0.0048(15)$ |
| 0.40000 | $-0.800020654976848$ | $+0.0108(16)$ |
| | $m_c = -0.800875(53 + 66)$ | |
| 0.45000 | $-0.906718750000000$ | $-0.0321(11)$ |
| 0.45000 | $-0.904988285480109$ | $-0.0179(14)$ |
| 0.45000 | $-0.903257820960218$ | $-0.0029(17)$ |
| 0.45000 | $-0.901697269855109$ | $+0.0277(22)$ |
| 0.45000 | $-0.900136718750000$ | $+0.0545(26)$ |
| | $m_c = -0.90377(06 + 49)$ | |
| 0.50000 | $-1.007094726562500$ | $-0.0130(19)$ |
| 0.50000 | $-1.006743165389559$ | $-0.0084(20)$ |

**Table B.4:** Continued.

| $g^2$ | $m$ | $\chi$ |
|---|---|---|
| 0.50000 | $-1.006391604216619$ | $-0.0069(20)$ |
| 0.50000 | $-1.005920411483309$ | $+0.0012(23)$ |
| 0.50000 | $-1.005449218750000$ | $+0.0109(25)$ |
| | $m_c = -1.006076(81 + 82)$ | |
| 0.55000 | $-1.110761718750000$ | $-0.0245(20)$ |
| 0.55000 | $-1.110045668023252$ | $-0.0160(24)$ |
| 0.55000 | $-1.109329617296505$ | $-0.0088(25)$ |
| 0.55000 | $-1.108400160210752$ | $+0.0118(31)$ |
| 0.55000 | $-1.107470703125000$ | $+0.0285(37)$ |
| | $m_c = -1.10907(08 + 16)$ | |

# Bibliography


[1] Ulli Wolff. Cluster simulation of relativistic fermions in two space- time dimensions. *Nucl. Phys.*, B789:258–276, 2008. arXiv:0710.2179.

[2] David J. Gross and Andre Neveu. Dynamical symmetry breaking in asymptotically free field theories. *Phys. Rev.*, D10:3235, 1974.

[3] Roger F. Dashen, Brosl Hasslacher, and Andre Neveu. Semiclassical Bound States in an Asymptotically Free Theory. *Phys. Rev.*, D12:2443, 1975.

[4] P. Forgacs, F. Niedermayer, and P. Weisz. The Exact mass gap of the Gross-Neveu model. 2. The 1/N expansion. *Nucl. Phys.*, B367:144–157, 1991.

[5] U. Wolff. THE PHASE DIAGRAM OF THE INFINITE N GROSS-NEVEU MODEL AT FINITE TEMPERATURE AND CHEMICAL POTENTIAL. *Phys. Lett.*, B157:303–308, 1985.

[6] Sinya Aoki and Kiyoshi Higashima. The Recovery of the Chiral Symmetry in Lattice Gross-Neveu Model. *Progress of Theoretical Physics*, 76(2):521–537, 1986.

[7] Ulli Wolff. Continuum limit of the lattice Gross-Neveu model with Wilson fermions. , 2008. In preparation.

[8] Walter E. Thirring. A soluble relativistic field theory. *Annals Phys.*, 3: 91–112, 1958.

[9] H. Bergknoff and H. B. Thacker. Structure and Solution of the Massive Thirring Model. *Phys. Rev.*, D19:3666, 1979.

[10] Pietro Rossi and Ulli Wolff. LATTICE QCD WITH FERMIONS AT STRONG COUPLING: A DIMER SYSTEM. *Nucl. Phys.*, B248:105, 1984.

[11] Christof Gattringer. Loop representation for 2-D Wilson lattice fermions in a scalar background field. *Nucl. Phys.*, B543:533–542, 1999. hep-lat/9811014.

[12] Shailesh Chandrasekharan and Uwe-Jens Wiese. Meron-cluster solution of a fermion sign problem. *Phys. Rev. Lett.*, 83:3116–3119, 1999. cond-mat/0201360.

[13] Tomasz Korzec and Ulli Wolff. Gross-Neveu model as a laboratory for fermion discretization. *PoS*, LAT2006:218, 2006. hep-lat/0609022.

[14] Tomasz Korzec. *Precise determination of universal finite volume observables in the Gross-Neveu model.* PhD thesis, Humboldt-Universität zu Berlin, 2007. http://nbn-resolving.de/urn:nbn:de:kobv:11-10078995.

[15] István Montvay and Gernot Münster. *Quantum Fields on a Lattice.* Cambridge University Press, 1994.

[16] Christof Gattringer, Verena Hermann, and Markus Limmer. Fermion loop simulation of the lattice Gross-Neveu model. *Phys. Rev.*, D76: 014503, 2007. arXiv:0704.2277.

[17] Ulli Wolff. Wilson fermions as a loop gas and their cluster simulation beyond two dimensions. Unpublished, 2008.

[18] R. Ben-Av, D. Kandel, E. Katznelson, P. G. Lauwers, and S. Solomon. CRITICAL ACCELERATION OF LATTICE GAUGE SIMULATIONS. *J. Statist. Phys.*, 58:125–139, 1990.

[19] Robert H. Swendsen and Jian-Sheng Wang. Nonuniversal critical dynamics in Monte Carlo simulations. *Phys. Rev. Lett.*, 58:86–88, 1987.

[20] Ulli Wolff. Collective Monte Carlo Updating for Spin Systems. *Phys. Rev. Lett.*, 62:361, 1989.

[21] William H. Press, Saul A. Teukolsky, William T. Vetterling, and Brian P. Flannery. *Numerical Recipes in C.* Cambridge University Press, 1992.

[22] Pierre L'Ecuyer. Maximally Equidistributed Combined Tausworthe Generators. *Math. Comp.*, 65:203 – 213, 1996.

[23] Makoto Matsumoto and Takuji Nishimura. Mersenne twister: a 623-dimensionally equidistributed uniform pseudo-random number generator. *ACM Trans. Model. Comput. Simul.*, 8(1):3–30, 1998.

[24] Martin Lüscher. A portable high-quality random number generator for lattice field theory simulations. *Computer Physics Communications*, 79 (1):100–110, 1994. hep-lat/9309020.

[25] F. James. RANLUX: A Fortran implementation of the high-quality pseudorandom number generator of Lüscher. *Computer Physics Communications*, 79(1):111–114, 1994.

[26] Oliver Bär and Ulli Wolff. Chiral symmetry at vanishing partition funtion in two dimensions. , 2008. In preparation.

[27] Björn Leder and Tomasz Korzec. Perturbative renormalisation of the chiral Gross-Neveu model. *PoS*, LAT2005:266, 2006. hep-lat/0509144.

[28] Nikolay Prokof'ev and Boris Svistunov. Worm algorithms for classical statistical models. *Phys. Rev. Lett.*, 87(16):160601, 2001.

[29] Ulli Wolff. Simulating the All-Order Strong Coupling Expansion I: Ising Model Demo. , 2008. arXiv:0808.3934.

[30] Ulli Wolff. Simulating the All-Order Hopping Expansion II: Wilson Fermions. , 2008. arXiv:0812.0677.

# Acknowledgement

First of all, I want to thank Ulli Wolff for providing this very interesting topic, for patiently (and sometimes repeatedly) discussing every single question I came up with, and for enabling me to participate so closely in his own research. I am indebted to Oliver Bär, who initially asked me to come to the Computational Physics group, and to Stefan Schaefer, who taught me a lot about programming. Oliver Witzel helped out in so many occasions, that it is impossible to name them all. It was a great pleasure to spend uncounted hours working, discussing, and chatting with Benedikt Biedermann. All the other members of the Computational Physics group, including Fatih Tekin, Shinji Takeda, Andreas Furchner, and Andrei Kramer were very important for making it a pleasure to work in this group.

# Selbstständigkeitserklärung

Hiermit erkläre ich, die vorliegende Arbeit selbstständig, ohne fremde Hilfe und nur unter Verwendung der angegebenen Literatur und Hilfsmittel verfasst zu haben.

Willi Rath, Berlin, 14. Januar 2009